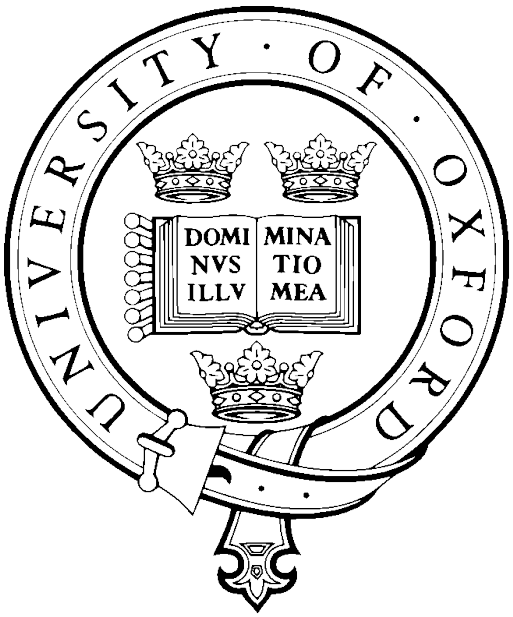
# Variability in Pigment Composition and Bio-optical Characteristics of Phytoplankton Populations in the Atlantic Basin

Sornsiri Phongphattarawat

A thesis submitted to the University of Oxford for the degree of
Master of Science by Research in Earth Sciences




Department of Earth Sciences and Linacre College
University of Oxford
2016

Supervised by Dr. Heather A. Bouman

# Abstract

Understanding sources of variability in the optical properties of phytoplankton and how the properties vary over the global ocean is essential in the development of ocean-colour algorithms to map the distribution of phytoplankton functional groups. Using data from oceanographic cruises covering different biogeochemical biomes and provinces over a broad latitudinal gradient of the Atlantic Basin, this study examined the spatial distribution of phytoplankton diagnostic pigments and absorption coefficients and how they varied with ocean observables (temperature and chlorophyll-a concentration) that can be detected from space. It was found that variation in the chlorophyll *a*-specific absorption coefficient of phytoplankton at 440 nm, $a_{ph}^{*}(440)$, was influenced significantly by changes in the proportion of the non-photosynthetic pigment (NPP), whereas pigment indices of cell size showed only a weak correlation with $a_{ph}^{*}(440)$. There were province- and biome-specific changes in the relationships between both temperature and chlorophyll $a$ and $a_{ph}^{*}(440)$. This suggests that when developing remote-sensing algorithms that use temperature or chlorophyll as a predictor of phytoplankton size structure, the underlying physical oceanographic processes that control the biogeochemistry and ecology of the region should be taken into consideration.

## Acknowledgements

First and foremost, I would like to express my deepest gratitude to my supervisor, Dr. Heather Bouman, who kindly accepted me as her student and introduced me to the world of biological oceanography. Throughout the year, she has been a constant source of inspiration, advice, and assistance, and has patiently guided me not only through data analysis but also through my writing. Also, I would like to thank Ms. Priscila Lange for her essential aid in the use of R, and thank the departmental academic administrators, in particular Ms. Elaine Sherrott, for their continued assistance in admissions and examination processes.

Bedford Institute of Oceanography, the British Oceanographic Data Centre, the Laboratoire d'Océanographie de Villefranche, the Japan Agency for Marine-Earth Science and Technology, and the Scottish Association for Marine Science are acknowledged for providing oceanographic data which have been used in this project. I would also like to acknowledge the full scholarship for my postgraduate education given by the Royal Thai Government via the Development and Promotion of Science and Technology Talents (DPST) Project. Thanks to the Department of Earth Sciences and Linacre College for ideal learning and living environment and facilities they have provided.

Finally, I would like to thank my parents, my brother, and my friends for their love and support throughout this difficult year, rebuilding my lost confidence when I had almost given up.

# Contents


Abstract 1

Acknowledgements 2

Contents 3

List of Figures 5

List of Tables 7

List of Abbreviations 8

**1. Introduction** 10

**2. Background** 13

2.1 Phytoplankton size classes and their major constituents 13

2.1.1 Picophytoplankton 14

2.1.2 Nanophytoplankton 15

2.1.3 Microphytoplankton 16

2.1.3.1 Diatoms (Bacillariophytes) 16

2.1.3.2 Dinoflagellates 17

2.2 Methods used to assess the oceanographic distribution of phytoplankton size classes 18

2.2.1 Size-fractionated chlorophyll *a* 18

2.2.2 Pigment markers (HPLC method) 20

2.3 Phytoplankton optical properties 22

2.3.1 Inherent optical properties 22

2.3.2 Variability in phytoplankton light absorption 24

2.3.2.1 Pigment composition 25

2.3.2.2 Pigment packaging 26

2.4 Objectives 28

**3. Methods** 29

3.1 Sampling procedures 30

3.2 Nutrient concentrations 31

3.3 Phytoplankton community structure 31

3.3.1 Phytoplankton pigment composition 31

3.3.2 Phytoplankton absorption 33

3.3.3 Phytoplankton pigment-based size classed 34

**4. Results** 37
4.1 Environmental variables and chlorophyll *a* concentration 37
4.2 Phytoplankton absorption coefficients 40
4.3 Effect of environmental factors on $a_{ph}^{*}(\lambda)$ 43
4.3.1 Temperature 44
4.3.2 Nutrient concentration 46
4.4 Effect of photoacclimation on $a_{ph}^{*}(\lambda)$ 47
4.5 Effect of phytoplankton community structure on $a_{ph}^{*}(\lambda)$ 51
**5. Discussion** 60
5.1 Effect of environmental factors on $a_{ph}^{*}(\lambda)$ 60
5.2 Effect of non-photosynthetic pigments on $a_{ph}^{*}(\lambda)$ 65
5.3 Distribution of size classes and its effect on $a_{ph}^{*}(\lambda)$ 69
**6. Conclusions and future work** 75
**References** 78

# List of Figures


| | | |
|---|---|---|
| Figure 2.1: | Schematic of HPLC analysis approach for characterising phytoplankton community structure on the basis of pigment composition. | 21 |
| Figure 2.2: | Interaction of light with a medium. | 23 |
| Figure 2.3: | Total absorption spectrum of an idealised, productive (1 mg chlorophyll *a* $m^{-3}$) oceanic water, together with spectra of the individual absorbing components. | 24 |
| Figure 2.4: | Assumed *in vivo* weight-specific absorption spectra of the main pigments, determined using absorption spectra of individual pigments in solvent. | 26 |
| Figure 2.5: | Effect of size and shape on light absorption properties of phytoplankton. | 27 |
| Figure 3.1: | Map showing sampling stations where phytoplankton absorption, pigment concentrations, and environmental variables were measured. | 29 |
| Figure 4.1: | Temperature plotted against TChl-*a* for surface (0-20 m) samples and histograms displaying the frequency distribution of the TChl-*a* and temperature. | 38 |
| Figure 4.2: | Nitrate ($[NO_2+NO_3]$) concentration for surface (0-20 m) samples plotted against TChl-*a* and temperature. | 38 |
| Figure 4.3: | Absorption coefficients for phytoplankton at 440 nm, $a_{ph}(440)$, plotted against TChl-*a* for surface samples. | 41 |
| Figure 4.4: | Chlorophyll *a*-specific absorption coefficients at 440 nm and 676 nm, $a^*_{ph}(440)$ and $a^*_{ph}(676)$, plotted against TChl-*a* for surface (0-20 m) samples. | 42 |
| Figure 4.5: | Chlorophyll *a*-specific absorption coefficients at 440 nm, $a^*_{ph}(440)$, plotted against temperature for surface (0-20 m) samples. | 45 |
| Figure 4.6: | Chlorophyll *a*-specific absorption coefficients at 440 nm, $a^*_{ph}(440)$ plotted against $[NO_2+NO_3]$ for surface (0-20 m) samples. | 46 |
| Figure 4.7: | The non-photosynthetic pigment index (NPP) plotted against TChl-*a* for surface (0-20 m) samples. | 47 |

| | | |
|---|---|---|
| Figure 4.8: | The non-photosynthetic pigment index (NPP) plotted against (*a*) the daily PAR just below the surface, PAR($0^-$), (*b*) the vertical attenuation coefficient for PAR, $K_d$, for surface (0-20) samples, and (*c*) at depth of the sample, PAR(*z*). | 49 |
| Figure 4.9 | Chlorophyll-*a* specific absorption coefficients at 440 nm, $a_{ph}^*(440)$, plotted against non-photosynthetic pigment index (NPP) for surface (0-20 m) samples. | 51 |
| Figure 4.10: | Ternary plot showing the percent contribution of each of the three pigment-based phytoplankton size classes to total phytoplankton biomass (percent pico, nano, and microphytoplankton) for surface (0-20 m) samples. | 52 |
| Figure 4.11: | The percent contribution of micro- ($S_\mu$), nano- ($S_n$), and picophytoplankton ($S_n$) plotted against temperature for surface (0-20 m) samples. | 54 |
| Figure 4.12: | The percent contribution of micro- ($S_\mu$), nano- ($S_n$), and picophytoplankton ($S_n$) plotted against TChl-*a* for surface (0-20 m) samples. | 55 |
| Figure 4.13: | Chlorophyll *a*-specific absorption coefficients at 440 nm, $a_{ph}^*(440)$, plotted against the percent contribution of micro- ($S_\mu$), nano- ($S_n$), and picophytoplankton ($S_n$) for surface samples. | 57 |
| Figure 4.14: | The size index (SI) plotted against TChl-*a* for the surface (0-20 m) samples. | 58 |
| Figure 4.15: | Chlorophyll *a*-specific absorption coefficients at 440 nm, $a_{ph}^*(440)$, plotted against values of SI for surface (0-20 m) samples. | 59 |

# List of Tables


| | | |
|---|---|---|
| Table 2.1: | Classification of phytoplankton into three main size classes. | 14 |
| Table 2.2: | Phytoplankton pigment markers and their associated size classes. | 22 |
| Table 2.3: | Classification of main pigments determined using HPLC analysis. | 25 |
| Table 3.1: | Oceanographic cruises included in the database. | 30 |
| Table 3.2: | Summary of the filtration volume, organic solvent, and reference for each method. | 32 |
| Table 3.3: | List of pigments detected in this study, along with their abbreviations, calculation, and their taxonomic significance. | 32 |
| Table 3.4 | Summary of the filtration volume, equipment, and β-correction algorithms used to measure phytoplankton absorption for each oceanographic cruise. | 34 |
| Table 4.1 | Values of numerical coefficients *A* and *B* of a power function relating phytoplankton absorption coefficient at 440 nm to TChl-*a* in the form $a_{ph}(440) = A[\text{TChl-}a]^B$. | 41 |

# List of Abbreviations

| Abbreviation | Description | Unit |
|---|---|---|
| ARCT | Atlantic Arctic Province | |
| BENG | Benguela Current Coastal Province | |
| BPLR | Boreal Polar Province | |
| BRAZ | Brazil Current Coastal Province | |
| CARB | Caribbean Province | |
| CDOM | Coloured dissolved organic matter | |
| CNRY | Canary Coastal Province | |
| DP | Sum of the weighted concentrations of all diagnostic pigments | mg $m^{-3}$ |
| EAFR | Eastern Africa Coastal Province | |
| FKLD | Southwest Atlantic Shelves Province | |
| GFST | Gulf Stream Province | |
| HNLC | High-nitrate, low-chlorophyll | |
| HPLC | High Performance Liquid Chromatography | |
| NARD | North Atlantic Drift Province | |
| NATR | North Atlantic Tropical Gyral Province | |
| NPP | Non-photosynthetic or photoprotective pigment index (the ratio of the concentration of non-photosynthetic pigments to total pigment concentration) | |
| NWCS | Northwest Atlantic Shelves Province | |
| PAR | Photosynthetically available radiation | mol photons $m^{-2}$ $day^{-1}$ |
| PAR($0^-$) | Daily PAR just below the surface | mol photons $m^{-2}$ $day^{-1}$ |
| PAR($z$) | Daily PAR at depth ($z$) of the sample | mol photons $m^{-2}$ $day^{-1}$ |
| SANT | Subantarctic Province | |
| SARC | Atlantic Subarctic Province | |
| SATL | South Atlantic Gyral Province | |
| SST | Sea-surface temperature | |
| SSTC | South Subtropical Convergence Province | |
| SI | Size index | μm |
| TChl-*a** | Total chlorophyll *a* (chlorophyll *a* + divinyl chlorophyll *a* + chlorophyllide *a*) | mg Chl-*a* $m^{-3}$ |
| $[NO_2+NO_3]$ | Nitrate (nitrite + nitrate) concentration | μM |
| $a(\lambda)$ | Total absorption coefficient of seawater at wavelength λ | $m^{-1}$ |
| $a_c(\lambda)$ | Absorption coefficient of CDOM at wavelength λ | $m^{-1}$ |
| $a_d(\lambda)$ | Absorption coefficient of extracted detrital material at wavelength λ | $m^{-1}$ |
| $a_{ph}(\lambda)$ | Absorption coefficient of phytoplankton at wavelength λ | $m^{-1}$ |
| $a_p(\lambda)$ | Absorption coefficient of total particulates retained on the sample filter at wavelength λ | $m^{-1}$ |
| $a_n(\lambda)$ | Absorption coefficient of inorganic (non-algal) particulate materials at wavelength λ | $m^{-1}$ |
| $a_w(\lambda)$ | Absorption coefficient of water at wavelength λ | $m^{-1}$ |
| $a^*_{ph}(\lambda)$ | Chlorophyll *a*-specific absorption coefficient of phytoplankton at wavelength λ | $m^2$ (mg Chl-*a*)$^{-1}$ |
| $a^*_{sol}$ | Weight-specific absorption coefficients of individual pigments | $m^2$ $mg^{-1}$ |
| $O_d(\lambda)$ | Optical density of extracted detrital material at wavelength λ | |
| $O_p(\lambda)$ | Optical density of total particulates retained on the sample filter | |
| $I_S$ | Geometric path length | m |
| $K_d$ | Vertical attenuation coefficient for PAR | $m^{-1}$ |
| $S$ | Clearance area of the sample filter | $mm^2$ |
| $V$ | Volume of seawater filtered | $m^3$ |

| Abbreviation | Description | Unit |
|---|---|---|
| $\beta$ | Optical path-length amplification factor | Dimensionless |
| $S_\mu$ | Percent contribution of microphytoplankton to Chl-*a* biomass | |
| $S_n$ | Percent contribution of nanophytoplankton to Chl-*a* biomass | |
| $S_p$ | Percent contribution of picophytoplankton to Chl-*a* biomass | |
| $z$ | Depth | m |

* Notation of other diagnostic pigments used in this study can be found in Table 3.3

# 1. Introduction

Marine phytoplankton are unicellular photoautotrophic organisms which play central roles in ocean ecosystems and global biogeochemical cycles. Through the process of photosynthesis, phytoplankton fix approximately 50 billion metric tonnes of organic carbon annually (Falkowski 1994; Field 1998), and thereby, contribute to the majority of marine primary production (Kirk 1994). This fixed organic carbon is then transferred to higher trophic levels via grazing and eventually to the entire food web. The fate of this productivity, whether it is transported to the deep ocean by physical processes or sinking, or if it is remineralised through microbial activities at the ocean's surface has an impact on ocean biogeochemistry and on the way the ocean regulates the concentrations of atmospheric carbon dioxide (Moore et al. 2013; Agusti et al. 2015).

The estimation of global marine primary production requires the use of optical algorithms to retrieve phytoplankton biomass data from satellite ocean-colour sensors (Hoepffner & Sathyendranath 1991; Lutz et al. 1996; Bouman et al. 2000; Lohrenz et al. 2003). The reflectance signal measured by ocean-colour satellite is a function of light absorption by marine phytoplankton. Consequently, changes in phytoplankton absorption efficiency can lead to errors in estimation of phytoplankton biomass and primary production by remote sensing (Bricaud et al. 2004). Understanding of how absorptive properties of phytoplankton vary over the world ocean is essential for improving estimates of global marine primary production using ocean-colour satellites.

The chlorophyll-specific absorption coefficient $a_{ph}^{*}(\lambda)$ (the absorption coefficient of phytoplankton at wavelength λ normalised to the chlorophyll-*a* concentration), which is an important parameter in spectral models of primary production (Bouman et al. 2003), is influenced predominately by variations in pigment packaging, which is a function of cell size and intracellular pigment concentrations, and pigment composition (Morel & Bricaud 1981: Hoepffner & Sathyendranath 1991; Bricaud et al. 1995). Variability in $a_{ph}^{*}(\lambda)$ is also known to vary in response to changes in environmental conditions (temperature, underwater light field, and nutrient availability) (Fujiki & Taguchi 2002; Stramski et al. 2002; Bouman et al. 2003; 2005; Platt et al. 2005). There have been numerous studies on the variations in $a_{ph}^{*}(\lambda)$ influenced by changes in species composition and size structure of marine phytoplankton communities as well as changes in environmental conditions for different regions of the Atlantic Ocean (e.g. Bricaud et al. 1995; 2004; Lazzara et al. 1996; Bouman et al. 2000; Stuart et al. 2000; Barlow et al. 2002). However, these studies are regional in scope and none of them have examined data covering a large latitudinal gradient, including polar regions.

In this study, I will examine the variability of pigment composition and optical properties of phytoplankton using pigment and light absorption data collected from across the entire Atlantic Basin covering polar, tropical, upwelling, central gyre, and high-nutrient, low-chlorophyll (HNLC) regions. Specifically, I will examine the effects of pigment composition and the cell size (as revealed by the diagnostic pigment markers) on $a_{ph}^{*}$. By dividing the large dataset into different biogeochemical biomes and provinces, I will be able to examine the impact of large-scale physical forcing on the optical properties of phytoplankton. The results of this study will improve our ability to monitor the biogeography of global-significant phytoplankton groups in

the ocean based on their optical characteristics. Such information is critical for global primary production and biogeochemical models as well as for fisheries and marine resource management.

# 2. Background

## 2.1 Phytoplankton size classes and their major constituents

Although all phytoplankton are capable of carbon fixation, different groups differ in their biogeochemical roles (Acevedo-Trejos et al. 2015) and their response to physical forcing (IOCCG 2014). Such differences in the functional roles of phytoplankton can be attributed in part to their size (Finkel et al. 2010; Acevedo-Trejos et al. 2015). For example, picophytoplankton have near-negligible sinking rates and therefore their productivity is recycled by bacterioplankton within the upper water column, whereas larger phytoplankton have high sinking rates, which leads to a larger fraction of their fixed carbon reaching the deep ocean without being remineralised (Sarmiento & Gruber 2006). In addition, the geographic distributions of the dominant size classes tend to vary, with large phytoplankton flourishing in nutrient-rich environments, such as in coastal upwelling regions, whereas small picophytoplankton usually dominate in the areas where nutrients are limited, such as in the subtropical oceanic gyres and high-nutrient, low-chlorophyll (HNLC) regions (Finkel et al. 2010; Acevedo-Trejos et al. 2015). Since cell size is relevant to several metabolic and biogeochemical processes (Nair et al. 2008), it is considered one of the most important traits used in global biogeochemical and ecological modelling.

Phytoplankton are often catagorised into three main size classes as shown in Table 2.1: picophytoplankton (0.2-2 µm), nanophytoplankton (2-20 µm) and microphytoplankton (20-200 µm) (Sieburth et al. 1978). The dominant members of each size class and their ecological and biogeochemical functions are described below.

Table 2.1: Classification of phytoplankton into three main size classes. Modified from Sieburth et al. (1978)

| Size class | Size range | Representatives |
|---|---|---|
| Microphytoplankton | 20-200 µm | Most diatoms and dinoflagellates |
| Nanophytoplankton | 2-20 µm | Microflagellates (coccolithophores, cyanophytes, silicoflagellates) |
| Picophytoplankton | 0.2-2 µm | Cyanobacteria, tiny eukaryotic protists |

### 2.1.1 Picophytoplankton

This group of phytoplankton consists of picocyanobacteria and photosynthetic picoeukaryotes. The common cyanobacterial genera which usually dominate the tropical and temperate oceans include *Synechococcus* and *Prochlorococcus* (Morel et al. 1993; Partensky et al. 1999). These cyanobacteria have been intensively studied, and their significant contribution to total phytoplankton biomass and marine primary production in the oligotrophic open ocean is well known (Li et al. 1983; Partensky et al. 1999).

Although *Synechococcus* has a broad geographic range from the poles to the tropics, *Prochlorococcus* is restricted to warm, nutrient-limited regions of the tropical and subtropical oceans covering a latitudinal range of 40°S to 40°N (Partensky et al. 1999; Flombaum et al. 2013; Biller et al. 2014). These two sister genera also differ in their vertical distributions: *Synechococcus* often occupies the upper part of the euphotic zone, whereas *Prochlorococcus* can be found in abundance at depths up to 200 m. The dominance of *Prochlorococcus* in the oligotrophic ocean has been attributed to its high surface area-to-volume ratio, which allows

these cells to acquire nutrients under extreme nutrient limitation (Barton et al. 2014). The ability of *Prochlorococcus* to grow at the base of the euphotic zone has also been explained by its small cell size: smaller cell size is associated with increased light absorption efficiency (Morel & Bricaud 1981; Kirk 1975). This high absorption efficiency is further enhanced by the presence of divinyl chlorophyll *b* (Uitz et al. 2009), which allows the cells to harvest extremely low levels of blue light at the bottom of the photic zone in the oligotrophic ocean (Moore et al. 1995; Sathyendranath & Platt 2007).

Picophytoplankton are important contributors to regenerated production in the oligotrophic ocean (Claustre 1994). This is owing in part to the inability of several strains of the dominant picophytoplankter, *Prochlorococcus*, to use nitrate ($NO_3^-$) as a nitrogen source, and consequently their growth relies heavily on reduced forms of nitrogen, such as urea and ammonium ($NH_4^+$) (Moore et al. 1995; Johnson & Lin 2009).

### 2.1.2 Nanophytoplankton

The nanophytoplankton size class consists of various groups of haptophytes (including the coccolithophores) and cryptophytes (Jeffrey et al. 2011). The well-known coccolithophorid *Emiliania huxleyi*, occasionally forms very dense blooms which lead to a white discolouration of the surface ocean that can be detected by satellite (Tyrrell et al. 1999). The biogeochemical functions of coccolithophores are also notable, particularly in the carbon (organic and inorganic) and sulphur cycles. As marine calcifiers, coccolithophores utilise dissolved bicarbonate ions in the surface waters to construct their coccoliths (Nair et al. 2008). This process releases carbon dioxide to the surface ocean and the atmosphere (Robertson et al. 1994). After the death of these

organisms, their calcium carbonate plates can dissolve in the water column or be deposited as sediments on the seafloor. Also, certain species of coccolithophores and haptophytes, in particular *Phaeocystis* spp., (Stefels & van Boekel 1993; Shen et al. 2011) can produce an organic compound called dimethylsulfoniopropionate (DMSP) which undergoes bacteria-mediated transformations into a dimethysulfide (DMS) gas (Yoch 2002). This gas, when released to the atmosphere, has the potential to induce the formation of clouds and thus influence the Earth's climate (Charlson et al. 1987; Keller 1989).

### 2.1.3 Microphytoplankton

The two major groups of phytoplankton belonging to the microphytoplankton size class include diatoms and dinoflagellates.

#### 2.1.3.1 Diatoms (Bacillariophytes)

Diatoms are ubiquitously distributed throughout the world's oceans. Due to their ability to rapidly grow and reproduce, they frequently dominate phytoplankton communities during bloom conditions and account for up to half of the marine primary production during bloom events (Yool & Tyrrell 2003; Le Quéré et al. 2005; Sarthou et al. 2005). Apart from being important marine primary producers, diatoms are also key players in the ocean's silicon cycle and in the biological pump (Yool & Tyrrell 2003; Agusti et al. 2015). On the global scale, they are estimated to take up about 240 tetramole of silicon per annum (Tréguer et al. 1995) to build their siliceous cell walls, making them the most significant marine silicifying organisms (Nair et al. 2008). With relatively high sinking rates compared with other marine phytoplankton, diatoms are important contributors to global export production to the deep ocean. The accelerated sinking speed of diatoms results primarily from their large cell size (Williams &

Follows 2011). Grazing by herbivorous zooplankton such as copepods further increases the export efficiency of diatoms by packaging cellular carbon into larger particles through the formation faecal pellets (Smayda 1971). In the post-bloom period, senescent diatom cells may form dense aggregates which rapidly sink through the water column (Smayda 1971).

#### 2.1.3.2 Dinoflagellates

Dinoflagellates consist of both photoautotrophic and heterotrophic species (Taylor et al. 2008). The majority of them are free-living, but a few tropical species, such as those in the zooxanthellae group, are reported to live as endosymbionts with reef animals, including corals, clams, radiolarians, acantharians or foraminiferans (Jeffrey et al. 2011). Some dinoflagellates can use the flagella to capture prey and obtain nutrition from them. This extraordinary 'mixotrophic' mode of living helps the photosynthetic microorganisms to supplement their nutrition and is common in light- or nutrient-limited environments (Hammer & Pitchford 2005). Various species of marine dinoflagellates are also reported to contribute significantly to DMP and DMSP production in the natural environment (Turner et al. 1988; Caruana & Malin 2014). In subtropical oceans, dinoflagellates usually dominate the phytoplankton community during the summertime after the diatom blooms (Kremp et al. 2008). Some of them can produce various kinds of toxins which are harmful to marine animals and humans. As blooms of dinoflagellates, particularly those of *Karenia brevis* and *K. mikimotoi*, can strongly modify the colour of the surface waters (IOCCG 2014), there have been attempts to monitor the blooms of such dinoflagellates spatially and temporally, using measurements of optical properties of the ocean both *in situ* and by remote sensing (e.g. Cullen et al. 1997; Miller et al. 2006; Kurekin et al. 2014).

## 2.2 Methods used to assess the oceanographic distribution of phytoplankton size classes

Various *in situ* techniques are used for both qualitative and quantitative analyses of the size structure in natural phytoplankton assemblages. Light microscopy is a conventional technique used in the identification and enumeration of phytoplankton species (Nair et al. 2008). Even though this method is relatively inexpensive and easily accessible, it can be laborious, requires a high level of expertise, and can be prone to errors (Billington 1991). Also, small cells such as pico- and nanophytoplankton lack well-defined morphologies and are frequently misidentified or excluded from cell counts (IOCCG 2014). Epifluorescence and electron microscopes can be used to enumerate picophytoplankton (Maclsaac & Stockner 1993; Nair et al. 2008), but these instruments require a high level of skill to operate and are expensive to maintain. Because of these drawbacks, many oceanographers have used phytoplankton pigments and their optical characteristics to determine the taxonomic composition and size structure of phytoplankton communities. The advantages and disadvantages of these two approaches are described in the following sections.

### 2.2.1 Size-fractionated chlorophyll *a*

The most commonly-used way to partition phytoplankton contained within a seawater sample into different size classes is to do a series of sequential filtrations using filters with specific pore-diameters (IOCCG 2014). Given that virtually all phytoplankton have chlorophyll *a* as their major light harvesting pigment (Kirk 1994), the measured concentration of chlorophyll *a* extracted from phytoplankton cells retained on the filter can be used to estimate the biomass of different phytoplankton size classes. Despite its simplicity, size-fractionated filtration has some

limitations, including breakage of phytoplankton cells or colonies and filter clogging (Mullin 1965; Runge & Ohman 1982). Following sample filtration and pigment extraction, the chlorophyll *a* concentration in each fraction can be determined using either fluorometry (measuring chlorophyll fluorescence) or High Performance Liquid Chromatography (HPLC) (Holm-Hansen et al. 1965; Claustre 1994).

Fluorometry is the most common technique used for measuring chlorophyll *a* in seawater. Fluorescence occurs when after chlorophyll molecules are excited through light absorption at one wavelength and then immediately re-emit light at a longer wavelength, returning the molecule back to its ground state (Kirk 1994; Falkowski & Raven 2007). The fluorescence intensity, as measured by a device called a fluorometer, can then be converted into the concentration of chlorophyll *a* (Lorenzen 1966; Sauzède et al. 2015). Although fluorometry is less accurate than HPLC in assessing the chlorophyll *a* content in a sample (Holm-Hansen et al. 1965; Sauzède et al. 2015), it is still widely used, principally because it is less expensive and relatively easy to measure (IOCCG, 2014). Its high sensitivity also allows the detection of chlorophyll *a* in small volumes of seawater, making it suitable for shipboard use (Yentsch & Menzel 1963; Holm-Hansen et al. 1965; Lorenzen 1966). Fluorometers are now integrated into the CTD (conductivity, temperature, and depth) package and other autonomous ocean platforms such as profiling floats and gliders, facilitating the measurement of *in vivo* fluorescence in the water column (Sauzède et al. 2015).

### 2.2.2 Pigment markers (HPLC method)

Phytoplankton possess a variety of pigments to aid in light harvesting and to protect cells from excessive sunlight (Bidigare 2005). These pigments are categorised into three structurally distinct groups: the chlorophylls (*a*, *b* and *c*), the carotenoids and the biliproteins (Kirk 1994). Historically, studies of phytoplankton pigments were restricted to the measurement of chlorophyll biomass using fluorometric or spectrophotometric methods (Jeffrey & Vesk 1997). However, in the past few decades, development of the HPLC technique has enabled scientists to separate, identify, and quantify a vast array of accessory pigments (Figure 2.1) from both field samples and laboratory cultures (Jeffrey & Mantoura 1997). Since HPLC analysis relies on extraction of pigments in non-aqueous organic solvents (Garrido et al. 2011), using this technique to detect water-soluble biliproteins is not possible.

HPLC not only provides information on chlorophyll *a* concentration (both monovinyl- and divinyl-chlorophyll *a*), which is a proxy for phytoplankton biomass (Claustre 1994; Uitz et al. 2006), it can also detect other accessory pigments, some of which are taxon-specific and can be used as chemotaxonomic markers (Jeffrey & Vesk 1997). By linking phytoplankton taxa to their corresponding size class, as shown in Table 2.2, it is possible to estimate from HPLC pigment data of diagnostic pigments the contribution of each size class to pigment biomass (Vidussi et al. 2001; Uitz et al. 2006).

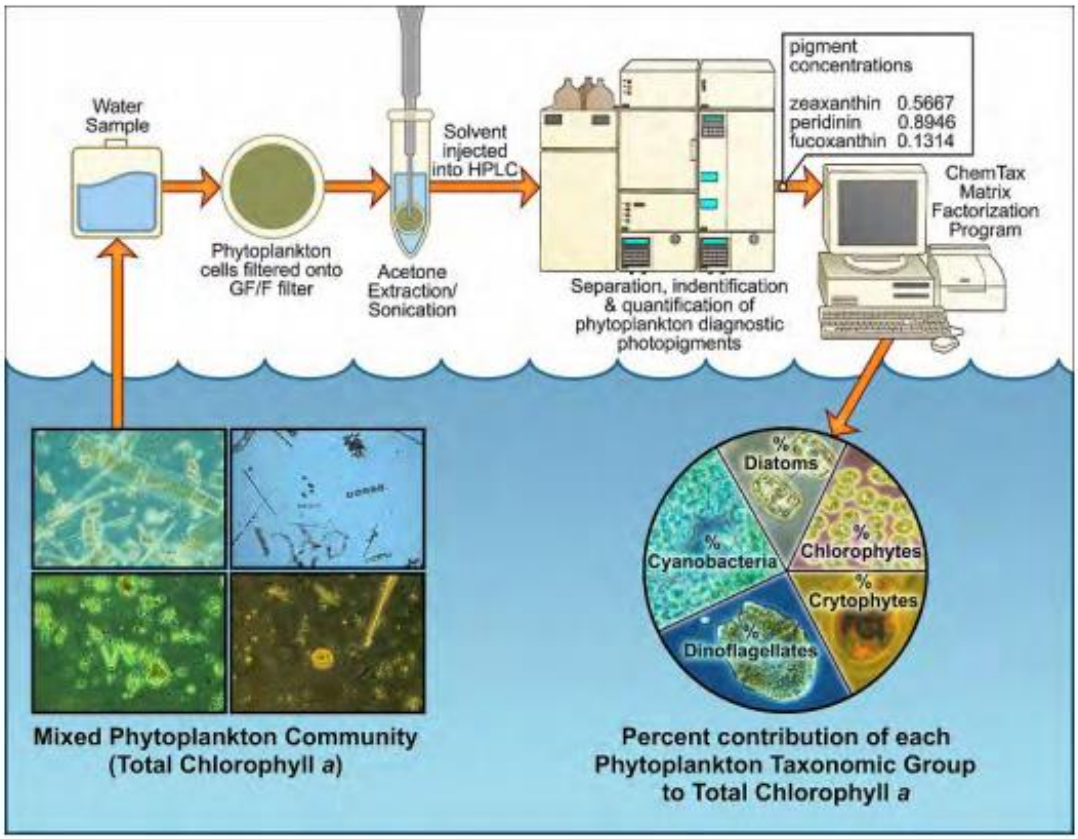



Figure 2.1: Schematic of HPLC analysis approach for characterising phytoplankton community structure on the basis of pigment composition. Mixed species natural samples are filtered, then extracted and injected into the HPLC system, where individual pigments are separated and quantified. From IOCCG (2014).

The HPLC method has its own set of limitations. First, HPLC analysis is costly and requires a high level of expertise when compared with bulk pigment methods. Second, large sample volumes are required for HPLC analysis to avoid missing minor accessory pigments (Bidigare et al. 2005). Third, difficulties in interpretation of pigment data may arise when pigment markers are common to several phytoplankton groups, and/or when they are contained within endosymbionts (Higgins et al. 2011).

Table 2.2: Phytoplankton pigment markers and their associated size classes. Modified from Vidussi et al. (2001) and Uitz et al. (2006).

| Pigments | Taxonomic significance | Size classes |
|---|---|---|
| **Chlorophylls** | | |
| Divinyl-chlorophyll *a* | *Prochlorococcus* | Picophytoplankton |
| Chlorophyll *b* + Divinyl chlorophyll *b* | *Prochlorococcus* and chlorophytes | Picophytoplankton |
| **Carotenoids** | | |
| Zeaxanthin | *Prochlorococcus* and cyanobacteria | Picophytoplankton |
| 19′-Hexanoyloxyfucoxanthin | Chromophytes and nanoflagellates | Nanophytoplankton |
| 19′-Butanoyloxyfucoxanthin | Chromophytes and nanoflagellates | Nanophytoplankton |
| Alloxanthin | Cryptophytes | Nanophytoplankton |
| Fucoxanthin | Diatoms | Microphytoplankton |
| Peridinin | Dinoflagellates | Microphytoplankton |

## 2.3 Phytoplankton optical properties

Phytoplankton both absorb and scatter light, and their bio-optical properties can be used to characterise phytoplankton communities in the surface ocean (Brewin et al. 2011). The following section provides background information regarding the concept of the inherent optical properties of phytoplankton and other seawater constituents and the factors governing absorptive properties of marine phytoplankton.

### 2.3.1 Inherent optical properties

When light, or more precisely a flux of photons, interacts with a medium such as water, it can be absorbed or scattered (Kirk 1994; Johnsen et al. 2011) (Figure 2.2.). The absorption and scattering properties of the medium are referred to as the inherent optical properties because they are characteristic of the medium itself, and do not depend on the ambient light field (Morel

& Bricaud 1986). The ability of the medium to absorb light can be quantified in terms of the absorption coefficient, which is defined as the ratio of the proportion of incident light absorbed light to the thickness of the medium (Kirk 1994).

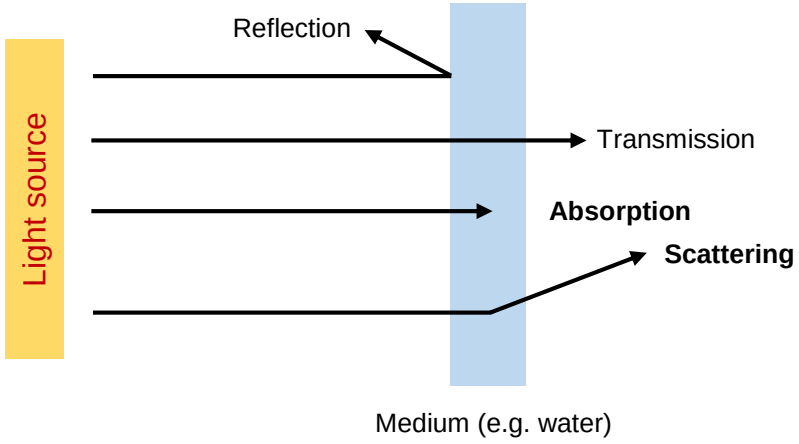



Figure 2.2: Interaction of light with a medium. Shown are the inherent optical properties of a medium (absorption and scattering) that are used in the studies of marine bio-optics. Modified from Kirk (1994).

In oceanic waters, there are four major components that contribute to light absorption: (1) the water itself, (2) phytoplankton, (3) coloured dissolved organic matter (CDOM), and (4) inorganic (or non-algal) particulate materials (Sosik 2008). The total absorption coefficient of seawater at any wavelength λ ($a(\lambda)$, $m^{-1}$), is a linear combination of the absorption coefficients of the four light-absorbing components:

$$a(\lambda) = a_w(\lambda) + a_{ph}(\lambda) + a_c(\lambda) + a_n(\lambda), \quad (2.1)$$

where the subscripts *w*, *ph*, *c*, and *n* represent water, phytoplankton, CDOM, and inorganic particulate materials, respectively (IOCCG 2006). The absorption spectra of the four light-absorbing components and the total absorption spectrum of seawater are shown in Figure 2.3.

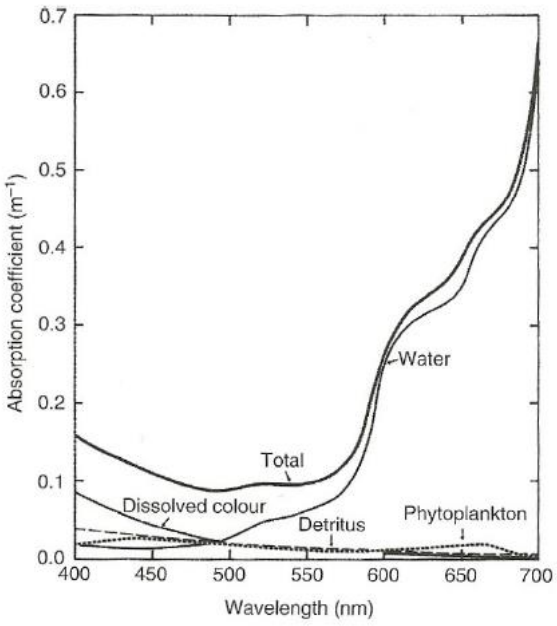



Figure 2.3: Total absorption spectrum of an idealised, productive (1 mg chlorophyll *a* $m^{-3}$) oceanic water, together with spectra of the individual absorbing components. From Kirk (1994).

For phytoplankton, which have chlorophyll *a* as a major pigment, it is common to normalise the absorption coefficient to the concentration of chlorophyll *a* ([Chl-*a*], mg Chl-*a* $m^{-3}$), to derive the chlorophyll *a*-specific absorption coefficient of phytoplankton ($a^*_{ph}(\lambda)$, $m^2$ (mg Chl-*a*)$^{-1}$) (Stuart et al. 2000; Morel 2008):

$$a^*_{ph}(\lambda) = \frac{a_{ph}(\lambda)}{[\text{Chl } a]}, \tag{2.2}$$

which can be considered a measure of the absorptive efficiency of phytoplankton cells.

### 2.3.2 Variability in phytoplankton light absorption

The absorptive properties of phytoplankton have often been used to infer information on the size structure and taxonomic composition of phytoplankton communities (Sosik 2008) on the

basis that the magnitude and the shape of phytoplankton absorption spectrum are influenced by two main factors: (1) intracellular pigment composition, and (2) pigment packaging (e.g. Bidigare et al. 1990; Hoepffner & Sathyendranath 1991; Bricaud & Stramski 1990; Stuart et al. 2000; Bricaud et al. 2004).

#### 2.3.2.1 Pigment composition

Phytoplankton pigments, as detected by the HPLC method, can be grouped into two main functional categories (Bidigare et al. 1990; Bouman et al. 2000): photosynthetic and non-photosynthetic (or photoprotective) pigments (Table 2.3). These pigments have different spectral absorption characteristics as illustrated in Figure 2.4. The total absorption spectrum of phytoplankton cells is the combined effect of individual pigments present in phytoplankton cells, each with its characteristic absorption spectrum (Sathyendranath et al. 1987; Bidigare et al. 1990). Pigment composition is known to vary amongst taxonomic groups of phytoplankton and with environmental factors regulating phytoplankton growth (Sosik 2008).

Table 2.3: Classification of main pigments determined using HPLC analysis. From Bouman et al. (2000)

| **Photosynthetic pigments** | **Non-photosynthetic pigments** |
|---|---|
| Chlorophyll *a* | Diadinoxanthin |
| Divinyl chlorophyll *a* | β-carotene |
| Chlorophyll *b* | α-carotene |
| Divinyl chlorophyll *b* | Zeaxanthin |
| Chlorophyll $c_1$, $c_2$, and $c_3$ | |
| Peridinin | |
| 19′-Hexanoyloxyfucoxanthin | |
| 19′-Butanoyloxyfucoxanthin | |
| Fucoxanthin | |

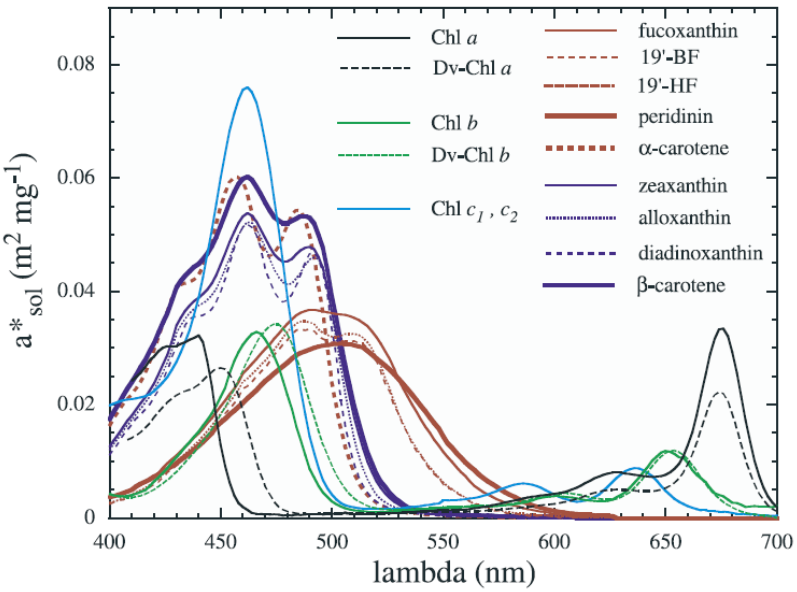



Figure 2.4: Assumed *in vivo* weight-specific absorption spectra of the main pigments, determined using absorption spectra of individual pigments in solvent. From Bricaud et al. (2004).

### 2.3.2.2 Pigment packaging

Pigments aggregated within phytoplankton cells or colonies are observed to have a lower specific absorption coefficient at all wavelengths and thus a flattened absorption spectrum, when compared with the equal amount of pigments uniformly dispersed in solution (Duyens 1956). This optical phenomenon is referred to as the pigment-packaging or the flattening effect. The degree of pigment-packaging is proportional to the cell size and shape, and intracellular pigment concentration (Bidigare et al. 1990; Bricaud et al. 2004). As the diameter of a cell increases, the pigment packaging becomes proportionally more pronounced. Consequently, absorption spectra for samples dominated by large microphytoplankton should appear flatter than those of smaller size classes (Ciotti et al. 2002). Conversely, if spherical cells were transformed into long, thin, cylindrical filaments randomly oriented, the pigment-packaging effect would be minimised (Kirk 1994). Figures 2.5*a*-*b* illustrate how the pigment-packaging

effect is altered through changes in cell size and shape. It is also important to note when examining these two figures, that the pigment-packaging effect is greatest at the peaks of the spectra where absorption is strongest (Kirk 1975; Morel & Bricaud 1986).

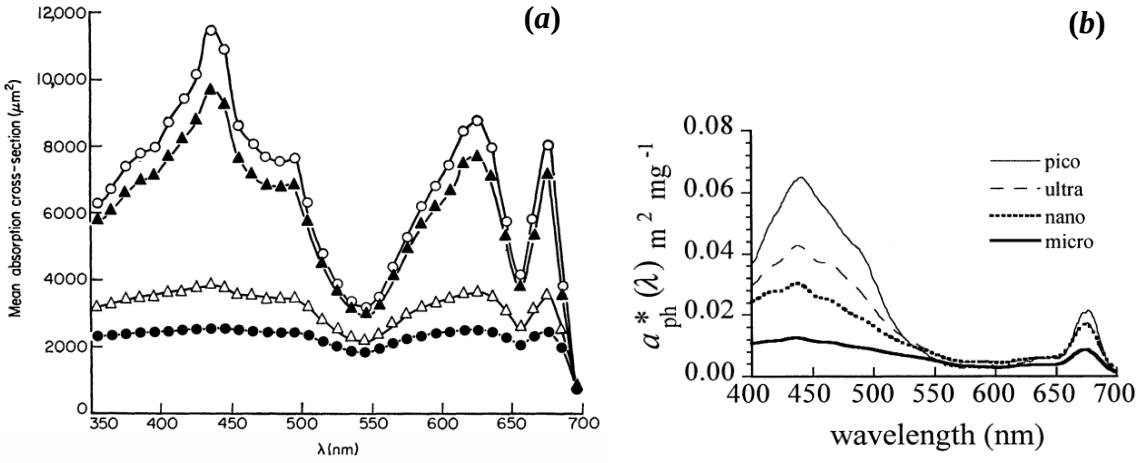



Figure 2.5: Effect of size and shape on light absorption properties of phytoplankton. (*a*) Mean absorption cross-section as a function of wavelength, for model blue-green algae of various shapes. In every case the data apply to 100,000 $\mu m^{-3}$ of algal volume, this corresponding to one particle in the case of the 57.6 μm diameter spheres (●), the 230.4 x 28.8 μm prolate spheroids (△), and the 3537 x 6 μm cylinders (▲); and to 884 particles in the case of the 6 μm diameter spheres (○). From Kirk (1976). (*b*) Spectral shape of average phytoplankton absorption coefficient normalised to chlorophyll *a* plus phaeopigments, for whole-water surface samples collected in all experiments, according to cell size range of the dominant organism. From Ciotti et al. (2002).

The intracellular pigment concentration can also influence pigment packaging. An increase in the concentration of pigment per cell is often due to a photoacclimatory response of phytoplankton cells to low-light conditions. In marine environments where light is strongly attenuated, such as during an intense bloom, phytoplankton deeper in the water-column acclimate to the low-light conditions by increasing their intracellular pigment concentration, which results in a corresponding flattening of the absorption spectrum (Stuart et al. 1998).

## 2.4 Objectives

Based on the background presented above, the aims of this study are:

1. By dividing the Atlantic dataset into biomes and provinces, to examine the impact of large-scale environmental factors on the community structure and absorption efficiency of phytoplankton.
2. Using pigment indices, to examine the effects of pigment composition and cell size on the absorptive properties of phytoplankton.

# 3. Methods

The database of phytoplankton absorption, pigment concentrations, and environmental variables used in this study was assembled from published observations made on oceanographic cruises covering different biomes and ecological provinces in the Atlantic Basin as defined by Longhurst (1998) (Figure 3.1 and Table 3.1).

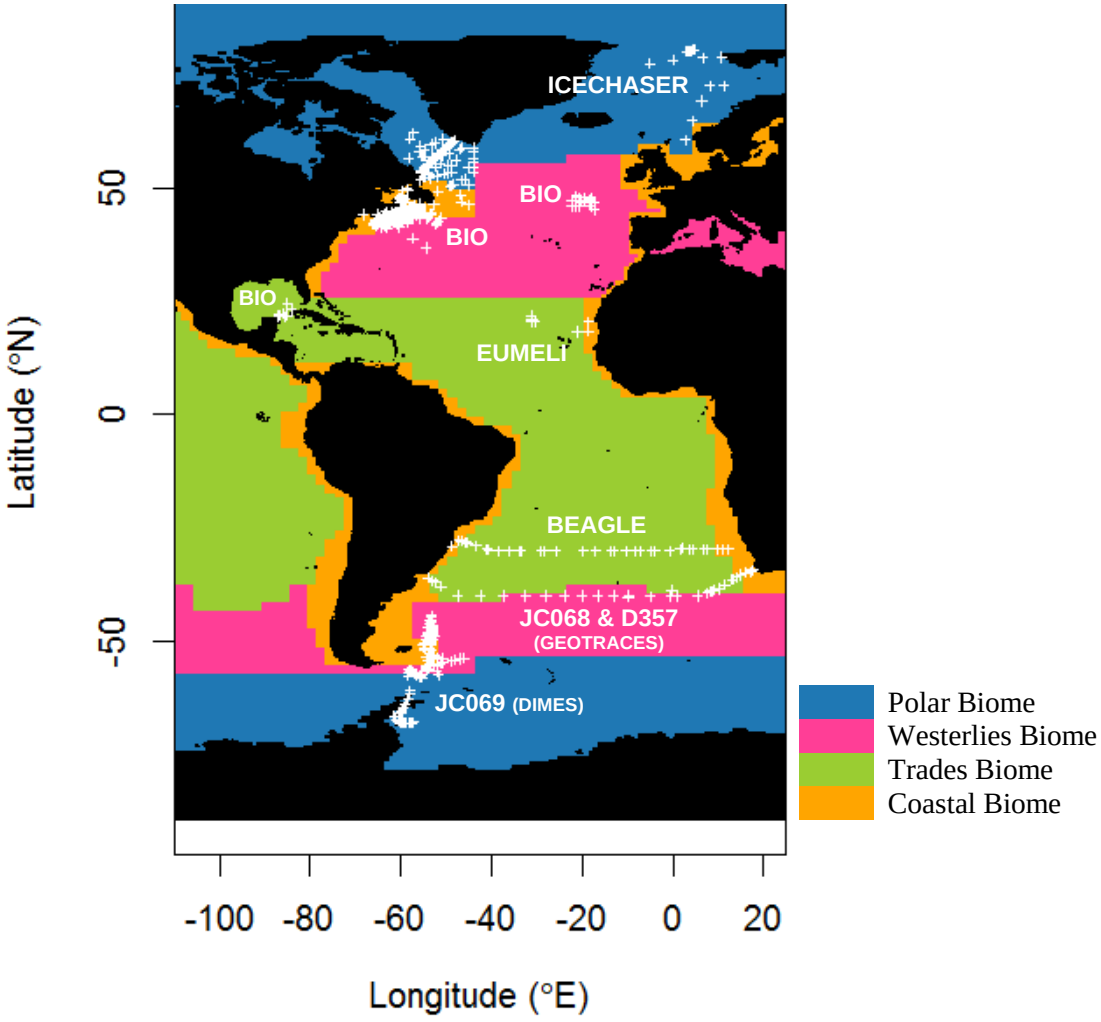



Figure 3.1: Map showing sampling stations where phytoplankton absorption, pigment concentrations, and environmental variables were measured. The Polar, Westerlies, Trades, and Coastal Biomes are shaded in blue, magenta, green, and orange, respectively.

## 3.1 Sampling procedures

At each station, seawater samples and environmental variables of interest were collected and recorded using a CTD (conductivity-temperature-depth) rosette system equipped with Niskin bottles. Samples for nutrient quantification were frozen and stored for analysis of nitrate, silicate, and phosphate concentration. Sampling depths and filtration volumes varied between cruises as summarised in Table 3.1.

Table 3.1: Oceanographic cruises included in the database. *N* is the number of samples collected from each cruise.

| **Cruise/Project** | **Location covered** | | **Year** | **Sampling depths (m)** | ***N*** | **Reference** |
|---|---|---|---|---|---|---|
| | **Biome** | **Province** | | | | |
| BIO | Polar<br>Westerlies<br>Trades<br>Coastal | BPLR; ARCT<br>NADR; GFST<br>CARB<br>NWCS | 1997-2003 | 0-130 | 1,091 | Stuart et al. (2000) |
| ICE-CHASER | Polar | BPLR; ARCT; SARC | June 2010 | 5-75 | 56 | Jackson (2013) |
| BEAGLE | Trades<br>Coastal | SATL<br>NWCS; BRAZ; BENG | 2003 | 10 | 34 | |
| EUMELI-3 | Trades | NATR | Oct. 1991 | 0-150 | 44 | Bricaud et al. (1995; 2004) |
| EUMELI-4 | Trades<br>Coastal | NATR<br>CNRY | June 1992 | 10-170 | * | Bricaud et al. (1995; 2004) |
| D357/UK-GEOTRACES | Westerlies<br>Trades<br>Coastal | SSTC<br>SATL<br>EAFR; BENG | Oct.-Nov. 2010 | 5-100 | 66 | Browning et al. (2014) |
| JC068/UK-GEOTRACES | Westerlies<br>Trades<br>Coastal | SSTC<br>SATL<br>EAFR; BENG | Dec. 2011-Jan. 2012 | 5-120 | 130 | Browning et al. (2014) |
| JC069/DIMES-UK3 | Polar<br>Westerlies<br>Coastal | APLR<br>SSTC; SANT<br>FKLD | Feb.-Mar. 2013 | 5, 20 | 103 | Browning et al. (2014) |

* For the EUMELI-4 cruise, data on phytoplankton absorption and pigment concentrations were collected at same station location and depth but separate casts. There were 25 samples collected for the measurement of absorption and 183 samples collected for the HPLC measurement of pigment concentrations.

## 3.2 Nutrient concentrations

For JC068 and D357 (GEOTRACES) and JC069 (DIMES) cruises, nitrate ([$NO_2$+$NO_3$]), silicate, and phosphate were quantified onboard using a 4-channel micromolar Bran and Luebbe AAIII segmented flow, colorimetric autoanalyser. Further details on the analytical methods are found in Woodward & Rees (2001). The results were standardised with a certified International Nutrient reference material provided by KANSO Technos, Japan. Nutrient analyses for EUMELI cruises were conducted onboard immediately following sample collections using a Technicon AutoAnalyser, according to the protocols of Wood et al. (1967) and Raimbault et al. (1990) for nitrate, and Murphy & Riley (1962) for phosphate and silicate. A Lachat QuickChem 8500 flow injection autoanalyser was used to carry out the measurements during ICECHASER cruise (Jackson 2013) using methods provided by the manufacturer.

## 3.3 Phytoplankton community structure

### 3.3.1 Phytoplankton pigment composition

Phytoplankton pigment composition was determined using HPLC analysis. Samples were vacuum filtered onto GF/F (glass-fibre) filters, flash frozen and stored in a -80$^{o}$C freezer until analysis. Subsequently, pigments were extracted in organic solvent and were analysed using a reverse-phase HPLC system. Table 3.2 summarises the filtration volume, organic solvents, and corresponding reference for each oceanographic dataset. Pigment identification was based on comparison of retention times and spectral absorption of individual pigments determined with known standards. Pigment concentrations were calculated from peak areas with a standard calibration method described in Bidigare (2013). The diagnostic HPLC pigments detected in this study are listed in Table 3.3.

Table 3.2: Summary of the filtration volume, organic solvent, and reference for each method used for HPLC pigment analysis for each oceanographic cruise.

| Cruise/Project | HPLC pigment analysis | | | Reference |
|---|---|---|---|---|
| | **Methodology** | **Filtered volume** | **Solvent used** | |
| BIO | Head & Horne (1993) | 100 mL | 90% acetone | Stuart et al. (2000) |
| ICECHASER | Barlow et al. (1997) | 0.2-1 L | 90% acetone | Jackson (2013) |
| BEAGLE | Head & Horne (1993) | 100 mL | 90% acetone | |
| EUMELI-3 | Claustre & Marty (1995) | 4 L | Methanol | Bricaud et al. (1995; 2004) |
| EUMELI-4 | Claustre & Marty (1995) | 2 L | Methanol | Bricaud et al. (1995; 2004) |
| D357 | Gibb et al. (2000) | 0.5-2 L | 90% acetone | Browning et al. (2014) |
| JC068 | Gibb et al. (2000) | 0.5-2 L | 90% acetone | Browning et al. (2014) |
| JC069 | Gibb et al. (2000) | 0.5-2 L | 90% acetone | Browning et al. (2014) |

Table 3.3: List of pigments detected in this study, along with their abbreviations, calculation, and their taxonomic significance. The main algal groups used here to describe the phytoplankton community composition are indicated in bold. Modified from Ras et al. (2008).

| Pigments | Abbreviation | Calculation | Taxonomic significance |
|---|---|---|---|
| Chlorophyll *a* | Chl-*a* | Chl-*a* + allomers + epimers | All phytoplankton, except *Prochlorococcus* |
| Divinyl Chlorophyll *a* | DVChl-*a* | | ***Prochlorococcus*** |
| Chlorophyllide *a* | Chld-*a* | Chld-*a* + Chld-*a*-like | Senescent diatoms |
| Total Chlorophyll *a* | TChl-*a* | Chl-*a* + DVChl-*a* + Chld-*a* | All |
| Chlorophyll *b* | Chl-*b* | | **Green algae** |
| Divinyl Chlorophyll *b* | DVChl-*b* | | ***Prochlorococcus*** |
| Total Chlorophyll *b** | TChl-*b* | Chl-*b* + DVChl-*b* | **Green algae, *Prochlorococcus*** |
| Chlorophyll $c_2$ | Chl-$c_2$ | | Various |
| Chlorophyll $c_3$ | Chl-$c_3$ | | **Prymnesiophytes**, Chrysophytes |
| Peridinin* | Peri | | **Dinoflagellates** |
| 19′-Hexanoyloxyfucoxanthin* | 19′-Hex | | **Prymnesiophytes** |
| 19′-Butanoyloxyfucoxanthin* | 19′-But | | **Pelagophytes**, Prymnesiophytes |
| Fucoxanthin* | Fuco | | **Diatoms,** Prymnesiophytes |
| Zeaxanthin* | Zea | | **Cyanobacteria, *Prochlorococcus*** |
| Alloxanthin* | Allo | | **Cryptophytes** |
| Diatoxanthin | Diat | | Various |
| Diadinoxanthin | Diad | | Various |
| Lutein | Lut | | **Chlorophytes** |
| Violaxanthin | Viola | | **Green algae** |
| Prasinoxanthin | Pras | | **Prasinophytes** |
| Carotene | Car | α-Car + β-Car | Various |

* Accessory pigments used in the determination of phytoplankton size classes according to Vidussi et al. (2001), Bricaud et al. (2004), and Uitz et al. (2009)

### 3.3.2 Phytoplankton absorption

Seawater samples for phytoplankton absorption measurements were filtered through glass-fibre (GF/F) filters. Optical densities of total particulates retained on the filters, $O_p(\lambda)$, were measured using a dual-beam spectrophotometer (model details see Table 3.4) equipped with an integrating sphere over the visible wavelengths (350-750 nm). A wetted GF/F filter paper (blank filter) was used as a reference. The optical densities of the total particulates were then converted to absorption coefficients, $a_p(\lambda)$ [$m^{-1}$], by dividing by the geometrical path length, $I_s$, which is the ratio of the volume of seawater filtered, $V$ [$m^3$], and the clearance area of the filter, $S$ [$mm^2$], and applying a correction for optical path-length amplification (β-correction factor) resulting from scattering by the filter (Bouman et al. 2000; Stuart et al. 2000). The absorption coefficient for total particulates, $a_p(\lambda)$, was calculated using the following equation:

$$a_p(\lambda) = \frac{2.3\ O_p}{\beta\ I_s}, \tag{3.1}$$

where 2.3 is the conversion factor for transforming common (base 10) logarithms to natural logarithms, and β is the β-correction factor derived at the various laboratories concerned (see Table 3.4).

The optical density of detrital material, $O_d(\lambda)$, was measured after extracting both the sample and the blank filters with hot methanol as described in Kishino et al. (1985). The absorption coefficients of detrital material, $a_d(\lambda)$, were determined by applying the same β-correction factor used in equation 3.1. Phytoplankton absorption coefficients, $a_{ph}(\lambda)$, were then obtained by

subtracting the detrital absorption spectra from the total absorption spectra (Stuart et al. 2000; Bricaud et al. 2004; Browning et al. 2014)

$$a_{ph}(\lambda) = a_p(\lambda) - a_d(\lambda). \quad (3.2)$$

The chlorophyll *a*-specific absorption coefficient of phytoplankton, $a^*_{ph}(\lambda)$, can then be calculated by normalising $a_{ph}(\lambda)$ to the HPLC-determined chlorophyll *a* concentration.

Table 3.4: Summary of the filtration volume, equipment, and β-correction algorithms used to measure phytoplankton absorption for each oceanographic cruise.

| Cruise/Project | Absorption measurement | | | Reference |
|---|---|---|---|---|
| | Filtered volume | Equipment | β-correction algorithm | |
| BIO | 100 mL | Shimadzu UV-2101 PC scanning spectrophotometer | Hoepffner & Sathyendranath (1992) | Stuart et al. (2000) |
| ICECHASER | 0.5-l L | Perkin Elmer Lambda 800 spectrophotometer | Hoepffner & Sathyendranath (1992) | Jackson (2013) |
| BEAGLE | 100 mL | Shimadzu UV-2101 PC scanning spectrophotometer | Hoepffner & Sathyendranath (1992) | |
| EUMELI-3 | 5-50 mL | LICOR 1800 UW spectroradiometer | Bricaud & Stramski (1990) | Bricaud et al. (1995; 2004) |
| EUMELI-4 | 5-50 mL | LICOR 1800 UW spectroradiometer | Bricaud & Stramski (1990) | Bricaud et al. (1995; 2004) |
| D357 | 0.5-1 L | Shimadzu UV-2550 spectrophotometer | Cleveland & Weidemann (1993) | Browning et al. (2014) |
| JC068 | 0.5-1 L | Shimadzu UV-2550 spectrophotometer | Cleveland & Weidemann (1993) | Browning et al. (2014) |
| JC069 | 0.5-1 L | Shimadzu UV-2550 spectrophotometer | Cleveland & Weidemann (1993) | Browning et al. (2014) |

### 3.3.3 Phytoplankton pigment-based size classes

Accessory pigments (chlorophylls *b*, *c* and carotenoids) are useful for analysing the taxonomic composition of phytoplankton communities, provided that the pigment in question is a distinct marker for a particular phytoplankton class or group. Diagnostic pigments used in this study

include fucoxanthin (Fuco), peridinin (Peri), alloxanthin (Allo), 19′-hexanoyloxyfucoxanthin (19′-Hex), 19′-butanoyloxyfucoxanthin (19′-But), zeaxanthin (Zea), and total chlorophyll *b* (TChl-*b*) (see Table 3.3 for details).

Claustre (1994), Vidussi et al. (2001), and Uitz et al. (2006) grouped phytoplankton taxa and their associated diagnostic pigments into three different size classes: picophytoplankton (0.2-2 µm), nanophytoplankton (2-20 µm), and microphytoplankton (20-200 µm). From concentrations of diagnostic pigments, the relative contributions of the three size classes to Chl-*a* biomass can be computed as follows (Bricaud et al., 2004):

$$S_p = \frac{0.86[\text{Zea}] + 1.01[\text{TChl-}b]}{\text{DP}} \times 100, \tag{3.3}$$

$$S_n = \frac{0.60[\text{Allo}] + 0.35[19'\text{-But}] + 1.27[19'\text{-Hex}]}{\text{DP}} \times 100, \tag{3.4}$$

$$S_\mu = \frac{1.41[\text{Fuco}] + 1.41[\text{Peri}]}{\text{DP}} \times 100, \tag{3.5}$$

where DP is the sum of the weighted concentrations of all diagnostic pigments:

$$\text{DP} = 1.41[\text{Fuco}] + 1.41[\text{Peri}] + 0.60[\text{Allo}] + 0.35[19'\text{-But}] + 1.27[19'\text{-Hex}] + 0.86[\text{Zea}] + 1.01[\text{TChl-}b]. \tag{3.6}$$

The numerical coefficients (weights) used in these equations were derived by conducting multiple linear regression analyses on a global HPLC-pigment database (Uitz et al. 2006).

As a single index to characterise the gross size structure of phytoplankton populations for analysing the relationships between phytoplankton size and environmental variables of interest, the 'size index (SI),' as proposed by Bricaud et al. (2004), was computed by assigning an average cell diameter to each size class (1 µm, 5 µm, and 50 µm for pico-, nano-, and microphytoplankton, respectively) and weighting the value by the relative contribution of each size determined using equations 3.3 to 3.5. The SI is expressed as:

$$\text{SI}\ (\mu\text{m}) \ = \ \frac{S_p + 5\ S_n + 50\ S_\mu}{100}. \qquad (3.7)$$

# 4. Results

## 4.1 Environmental variables and chlorophyll *a* concentration

The relationship between seawater temperature and HPLC-derived chlorophyll *a* concentration (TChl-*a*) for surface samples (0-20 m) is shown in Figure 4.1*a* along with the corresponding frequency distribution of each variable (Figures 4.1*b*, *c*). TChl-*a* varied from 0.03 to 13.9 mg $m^{-3}$ and the surface water temperatures ranged from -1.8ºC to 26.3ºC, with the majority of samples (71.5%) lying below 20ºC in polar and temperate regions of the Atlantic Basin. The relationship between surface [$NO_2$+$NO_3$] and TChl-*a* is shown in Figure 4.2*a*. [$NO_2$+$NO_3$] ranged from below the limit of detection to 27.8 µM, with data significantly skewed toward the lower range.

The three biogeochemical provinces located within the Trades Biome (South Atlantic Gyral (SATL), North Atlantic Tropical Gyral (NATR), and Caribbean (CARB)) were characterised by relatively warmer surface waters (10.0-26.3ºC), low biomass (TChl-*a* < 1.0 mg $m^{-3}$) and relatively low [$NO_2$+$NO_3$] (< 9.0 µM) (Figures 4.1 and 4.2). Provinces found within the Polar Biome (Boreal Polar (BPLR), Atlantic Arctic (ARCT), Atlantic Subarctic (SARC), and Austral Polar (APLR)) were characterised by colder waters (≤ 11.2ºC), with TChl-*a* and [$NO_2$+$NO_3$] showing a high degree of variation. The highest [$NO_2$+$NO_3$] was 27.8 µM and coincided with the lowest TChl-*a* (0.03 mg $m^{-3}$) in the APLR Province in the Southern Ocean, a high-nitrate, low-chlorophyll (HNLC) region. In contrast, the sample with the highest TChl-*a* (13.9 mg $m^{-3}$) belonged to the BPLR Province in the Arctic Ocean.

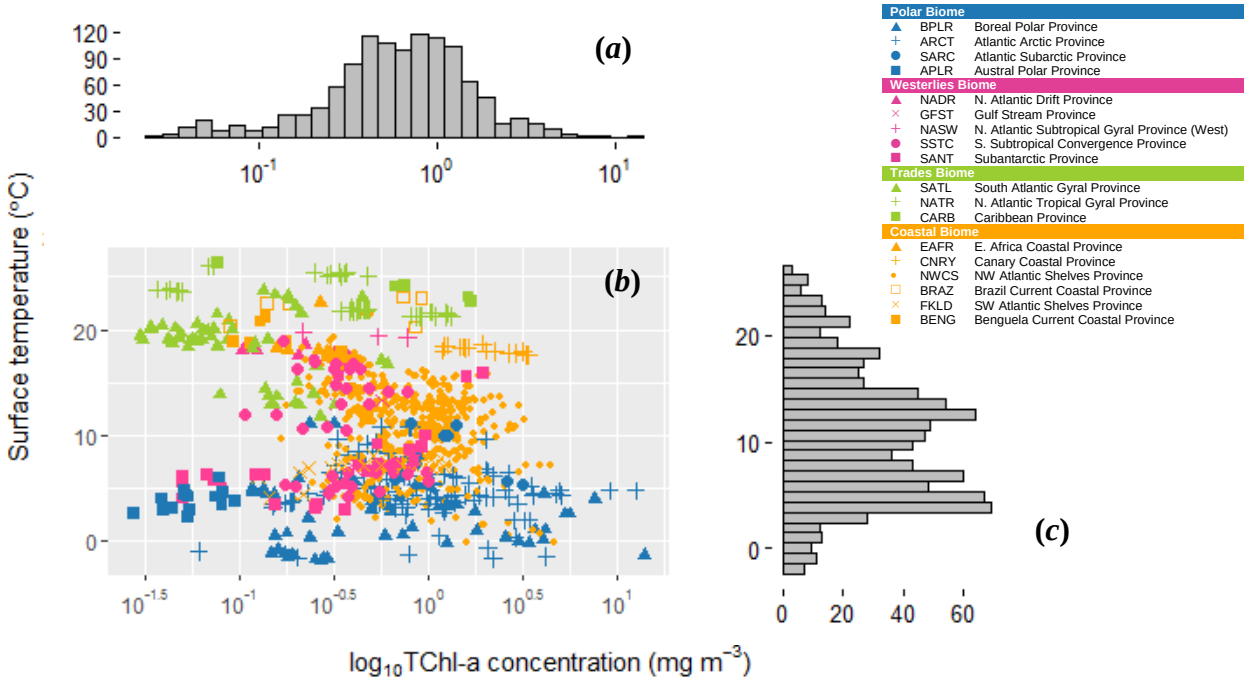



Figure 4.1: (*b*) Temperature plotted against TChl-*a* for surface (0-20 m) samples. (*a*,*c*) Histograms display the frequency distribution of the TChl-*a* and temperature. Colours and shapes are assigned according to biomes and provinces, respectively.

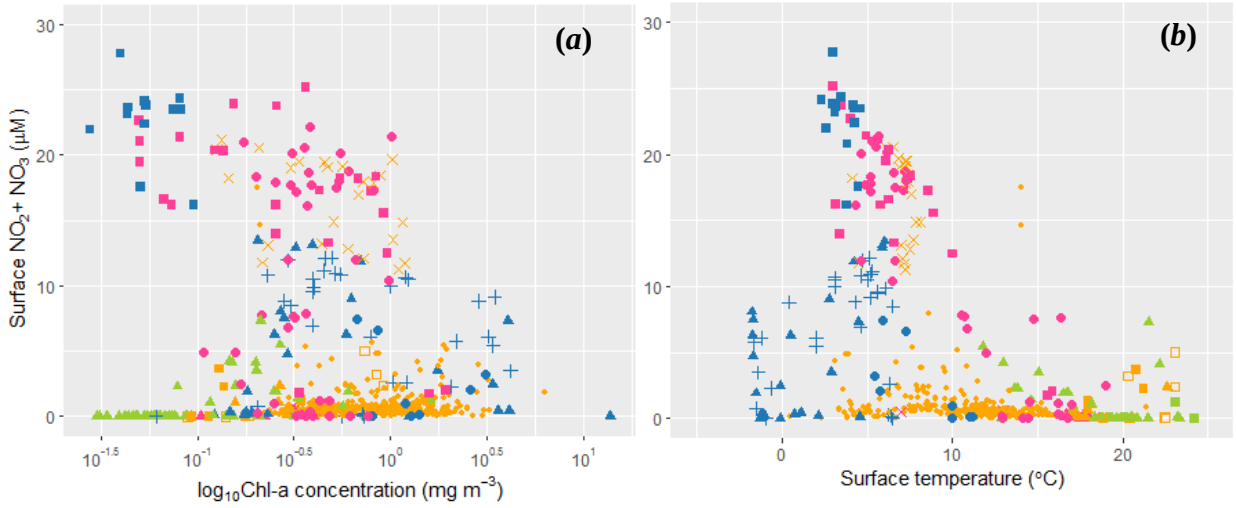



Figure 4.2: Nitrate ([$NO_2$+$NO_3$]) concentration for surface (0-20 m) samples plotted against (*a*) TChl-*a* and (*b*) temperature.

Environmental variables (temperature and [$NO_2$+$NO_3$]) and TChl-*a* were also highly variable within the Westerlies Biome. Samples tended to separate into two clusters (Figures 4.1 and 4.2): one with low temperature (< 10$^o$C) and low TChl-*a* (< 1 mg $m^{-3}$) corresponding to the western part (~50$^o$W) of the South Subtropical Convergence (SSTC) and the Subantarctic (SANT) Provinces, and another with high temperature (> 10$^o$C) and low TChl-*a*, which corresponded to the North Atlantic Drift (NADR) Province, the western North Atlantic Subtropical Gyral (NASW) Province, and eastern part (~0-40$^o$W) of the SSTC Province. In terms of nutrient availability, most of the samples from the SSTC and the SANT Provinces had high [$NO_2$+$NO_3$] (> 10.0 µM). Thus, these two provinces could be classified as HNLC.

The Coastal Biome spans a broad latitudinal range from the poles to the equator, which leads to a range in surface water temperatures. Coastal provinces in lower latitudes, including the Brazil Current Coastal (BRAZ), the Benguela Current Coastal (BENG), the East Africa Coastal (EAFR), and the Canary Coastal (CNRY) Provinces, exhibited elevated surface temperatures which exceeded 17$^o$C. In contrast, the Southwest Atlantic Shelves (FKLD) Province was characterised by cooler waters (< 8.2$^o$C). The Northwest Atlantic Shelves (NWCS) Province extends from ~42 to 50$^o$N, and the observed temperatures within this province varied from -0.1 to 20$^o$C. In general, surface samples taken from the Coastal Biome tended to have consistently low [$NO_2$+$NO_3$] (< 6.0 µM), except for those from the cold FKLD Province, which had [$NO_2$+$NO_3$] greater than 11.0 µM. The relationships between temperature, [$NO_2$+$NO_3$], and TChl-*a* in this biome showed a high degree of scatter, reflecting the dynamic and complex nature of this oceanographic regime.

Relationships between temperature and [$NO_2$+$NO_3$] relate to the large-scale chemical structure of the ocean (Switzer et al. 2003). Figure 4.2*b* illustrates the relationship between temperature and [$NO_2$+$NO_3$] for surface samples collected in this study. Inverse correlations were particularly evident in the Southern Ocean provinces APLR, SANT, and SSTC. For other biomes, there was a high degree of scatter in the relationship between temperature and [$NO_2$+$NO_3$] with a tendency for the arctic provinces to have elevated [$NO_2$+$NO_3$] at low temperatures.

## 4.2 Phytoplankton absorption coefficients

Several authors have described the relationship between TChl-*a* and $a_{ph}(440)$ using various linear and non-linear functions (Prieur & Sathyendranath 1981; Bricaud et al. 1995; 2004). In this study, the entire dataset was fitted using a power function and coefficients were compared with those obtained in the studies of Prieur & Sathyendranath (1981) and Bricaud et al. (2004), which used bio-optical data collected in different regions of the global ocean (Figure 4.3). Coefficient values obtained in this study (Table 4.1) were closer to those obtained by Prieur & Sathyendranath (1981) compared with those reported in Bricaud et al. (2004).

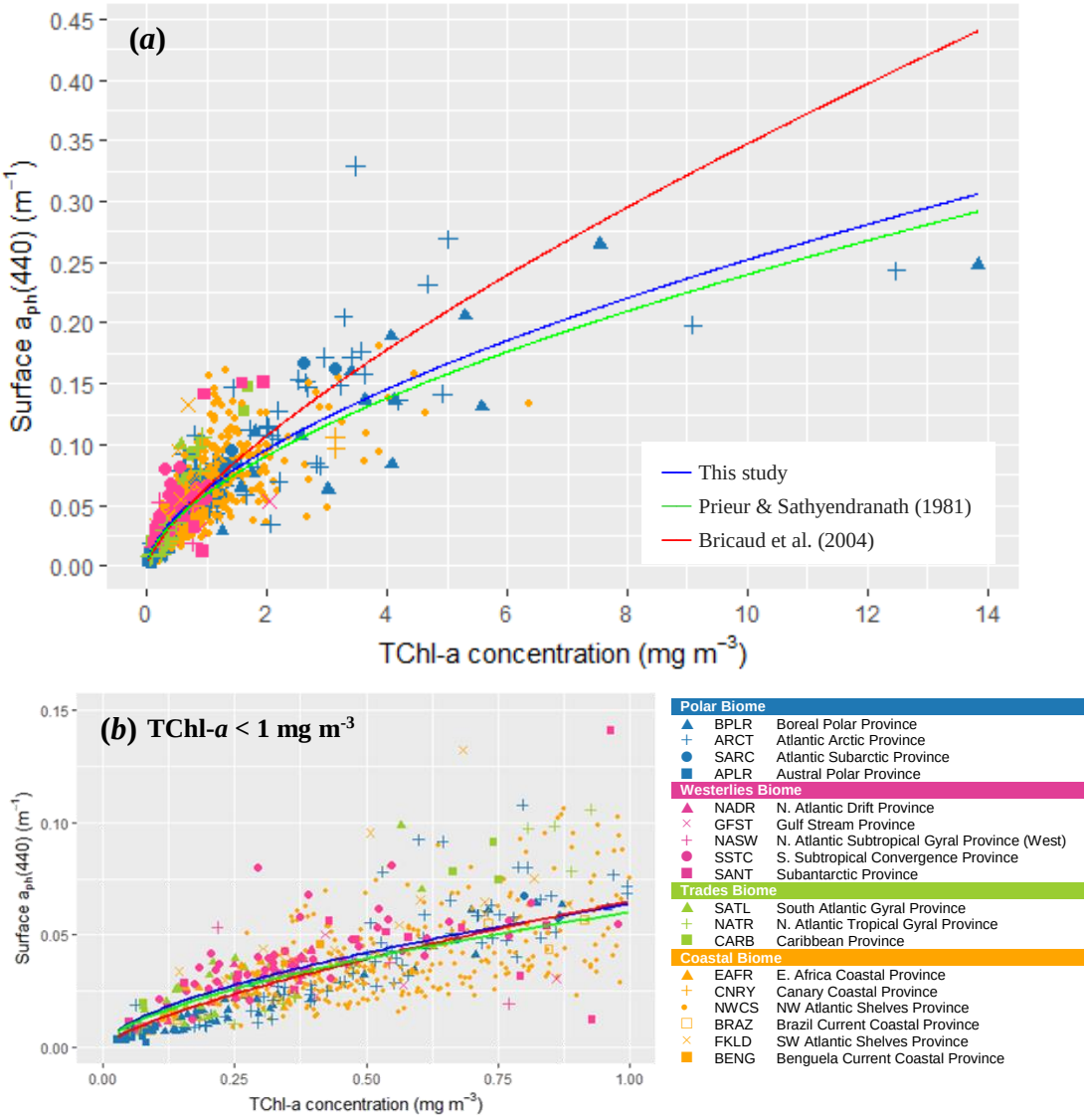



Figure 4.3: (*a*) Absorption coefficients for phytoplankton at 440 nm, $a_{ph}(440)$, plotted against TChl-*a* for surface samples. A power regression line fitted to the entire dataset is shown along with equations used in the studies of Prieur & Sathyendranath (1981) and Bricaud et al. (2004). (*b*) As Figure 4.3*a* for the samples with TChl-*a* less than 1 mg $m^{-3}$.

Table 4.1: Values of numerical coefficients *A* and *B* of a power function relating phytoplankton absorption coefficient at 440 nm to TChl-*a* in the form $a_{ph}(440) = A[\text{TChl-}a]^B$. *N* is the number of samples used in each study. *S.E.* is the standard error.

| **Studies** | ***N*** | ***A*** | ***B*** | $r^2$ | ***S.E.*** |
|---|---|---|---|---|---|
| This study | 1552 | 0.064 | 0.598 | 0.597 | 0.021 |
| Prieur & Sathyendranath (1981) | 40 | 0.060 | 0.602 | 0.922 | |
| Bricaud et al. (2004) | 596 | 0.065 | 0.728 | 0.934 | |

The chlorophyll *a*-specific absorption coefficients of phytoplankton, $a^*_{ph}(\lambda)$, were plotted against TChl-*a* for both blue (440 nm) and red (676 nm) peaks of phytoplankton absorption (Figure 4.4). The values of $a^*_{ph}(440)$ for the surface samples ranged from 0.01 to 0.31 $m^2$ (mg Chl-*a*)$^{-1}$, and those of $a^*_{ph}(676)$ from 0.005 to 0.112 $m^2$ (mg Chl-*a*)$^{-1}$. In general, $a^*_{ph}(\lambda)$ at both wavelengths decreased with increasing TChl-*a*, a trend that was particularly evident at the blue peak (440 nm).

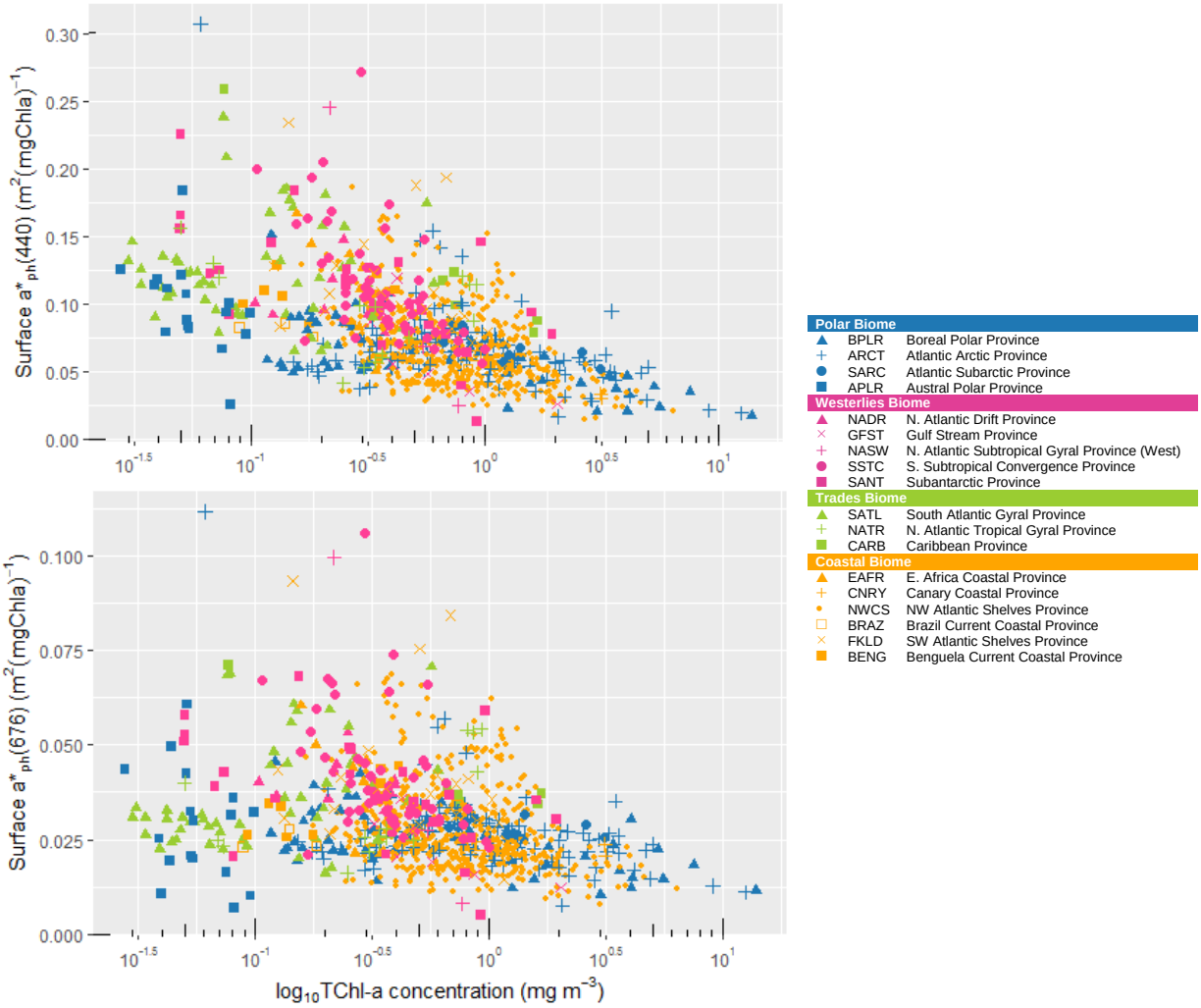



Figure 4.4: Chlorophyll *a*-specific absorption coefficients at 440 nm and 676 nm, $a^*_{ph}(440)$ and $a^*_{ph}(676)$, plotted against TChl-*a* for surface (0-20 m) samples.

With very few exceptions, samples from the Polar Biome showed consistently low $a_{ph}^{*}(\lambda)$ at both wavelengths ($a_{ph}^{*}(440) < 0.15$ and $a_{ph}^{*}(676) < 0.06$ m$^2$ (mg Chl-*a*)$^{-1}$) along the range of observed TChl-*a*. Another cluster of points with high $a_{ph}^{*}(\lambda)$ at both 440 and 676 nm and low TChl-*a* corresponds to samples from the SSTC, the SANT, the NASW (Westerlies Biome), the FKLD (Coastal) as well as the CARB and part of the SATL (Trades) Provinces. For absorption coefficients at the blue peak (440 nm), points corresponding to samples from the SATL Province cluster around different ranges of $a_{ph}^{*}(440)$ and TChl-*a* along both of these two curves. One cluster consisting of samples collected at ~30ºS in the SATL Province during the BEAGLE cruise had $a_{ph}^{*}(440)$ ranging from 0.075 to 0.15 m$^2$ (mg Chl-*a*)$^{-1}$, coinciding with TChl-*a* less than 0.1 mg m$^{-3}$. Another cluster contains samples obtained during the JC068 and DIMES cruises between the latitudes of ~36ºS and 40ºS. These samples had a wider range of $a_{ph}^{*}(440)$ from just above 0.05 to ~0.25 m$^2$ (mg Chl-*a*)$^{-1}$, corresponding to TChl-*a* values ranging between 0.1 and 1.0 mg m$^{-3}$.

## 4.3 Effect of environmental factors on $a_{ph}^{*}(\lambda)$

Given that this study includes data collected from a broad range of biogeochemical provinces from across the Atlantic Basin, it is expected that environmental variables such as temperature and nutrient concentration will vary widely. In this section, we examine how changes in temperature and nutrient availability are related to variations in phytoplankton absorption efficiency (Stuart et al. 2000; Bouman et al. 2003).

### 4.3.1 Temperature

The chlorophyll-specific absorption coefficients of marine phytoplankton have been shown to be positively correlated with temperature in the temperate waters of the Northwest Atlantic (Bouman et al. 2003; Platt et al. 2005). For this larger dataset, temperature (*T*) and $a_{ph}^{*}(440)$ exhibited a weak correlation ($a_{ph}^{*}(440) = 0.062 + 0.002T$, $r^2 = 0.069$, $p < 0.05$, $N = 757$) as shown in Figure 4.5*a*. However, some interesting patterns emerged when each ocean biome was examined separately (Figure 4.5*b*). For the Coastal Biome, values of $a_{ph}^{*}(440)$ showed a slight positive correlation with temperature over a range of 0 to 23°C ($a_{ph}^{*}(440) = 0.051 + 0.002T$, $r^2 = 0.067$, $p < 0.05$, $N = 406$). In contrast, the Trades Biome, in particular the SATL province, showed a negative correlation between temperature and $a_{ph}^{*}(440)$ ($a_{ph}^{*}(440) = 0.214 – 0.005T$, $r^2 = 0.214$, $p < 0.05$, $N = 72$).

A high degree of scatter in the relationship between temperature and $a_{ph}^{*}(440)$ was observed in the Westerlies Biome, especially at temperatures greater than 10°C. For temperatures below 10°C, $a_{ph}^{*}(440)$ values tended to decrease with increasing temperature, and this pattern was particularly distinct for stations located within the SSTC, the SANT, and the GFST Provinces. When compared with those from tropical and temperate biomes, values of $a_{ph}^{*}(440)$ for the Polar Biome are relatively low for both the Arctic and Southern Ocean provinces, and there is no observed significant correlation between temperature and $a_{ph}^{*}(440)$ for the relatively narrow range of temperature characterising this oceanic regime ($r^2 = 0.005$, $p = 0.33$, $N = 191$).

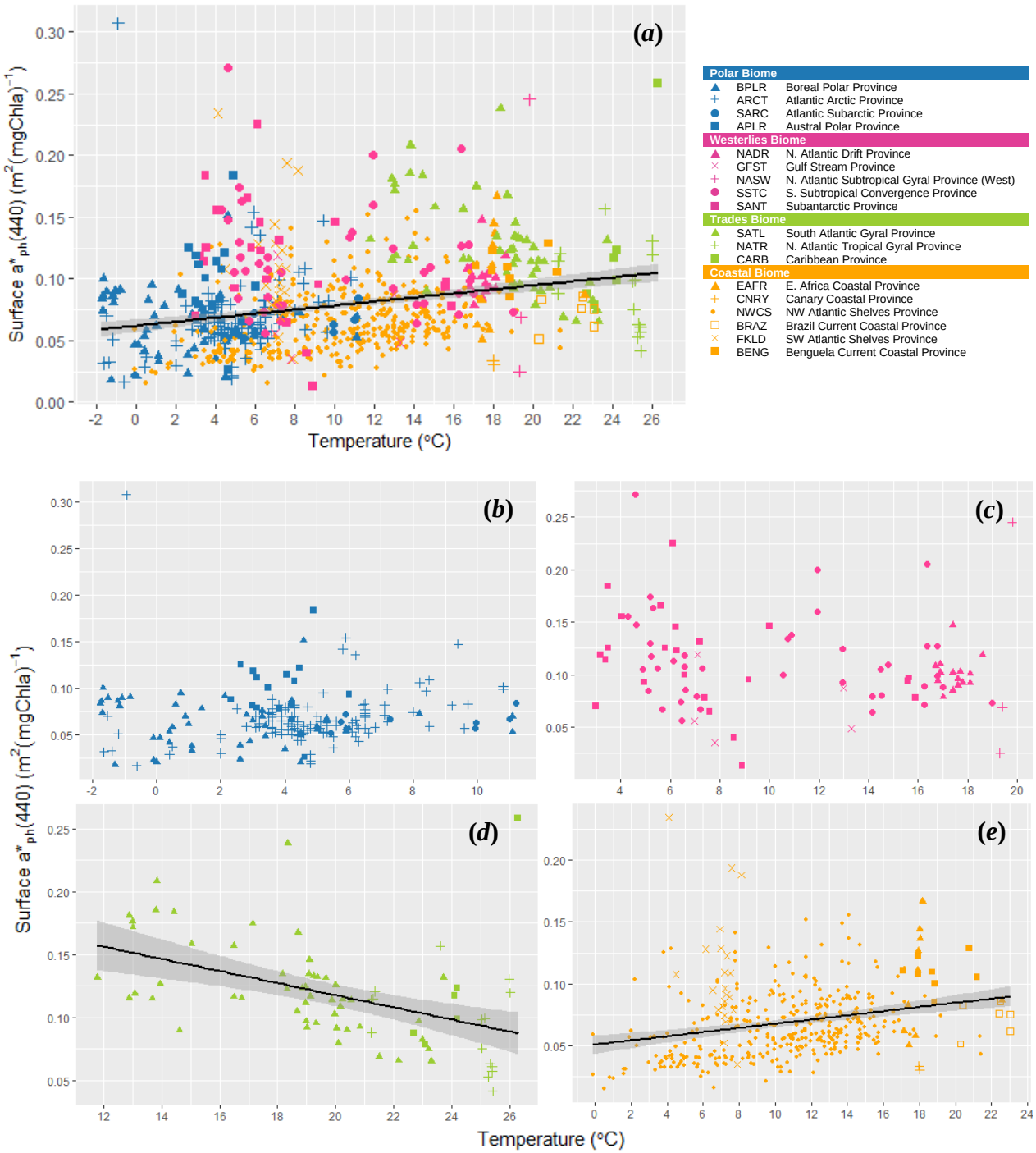



Figure 4.5: (*a*) Chlorophyll *a*-specific absorption coefficients at 440 nm, $a^*_{ph}(440)$, plotted against temperature for surface (0-20 m) samples. (*b*-*e*) As Figure 4.4*a* for each biome. Linear regression analyses were performed (black lines), and the 95% confidence intervals for the linear regression lines are shaded in gray.

### 4.3.2 Nutrient concentration

Nutrient availability is another environmental factor that has been related to the size structure (Platt et al., 2005) and absorptive properties (Sosik & Mitchell 1991; Stramski et al. 2002) of natural phytoplankton assemblages. To examine the relationship between nutrients and phytoplankton absorption in this study, $a^*_{ph}(440)$ was plotted as a function of [$NO_2$+$NO_3$] for the subset of data where information on [$NO_2$+$NO_3$] was available (N = 539; Figure 4.6). The plot shows a weak positive correlation between $a^*_{ph}(\lambda)$ and [$NO_2$+$NO_3$] ($a^*_{ph}(440)$ = 0.072 + 0.002[$NO_2$+$NO_3$], $r^2$ = 0.08, $p < 0.05$) especially for the Polar and Westerlies Biomes, although the considerable scatter did occur especially when [$NO_2$+$NO_3$] was low (< 5 µM).

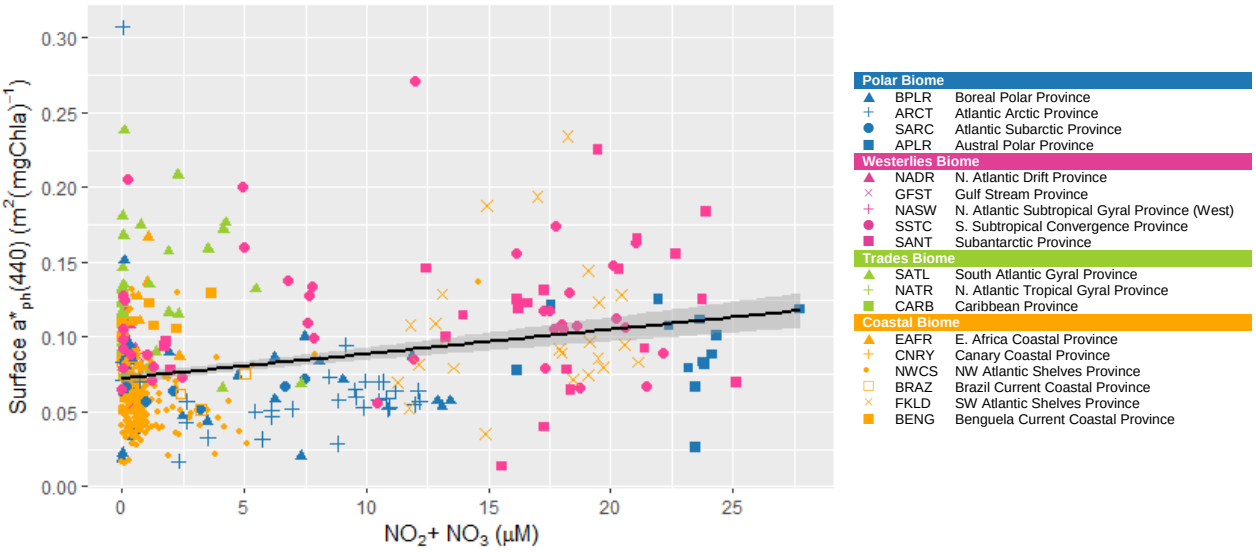



Figure 4.6: Chlorophyll *a*-specific absorption coefficients at 440 nm, $a^*_{ph}(440)$ plotted against [$NO_2$+$NO_3$] for surface (0-20 m) samples. The black line represents the line of best fit (equation with $r^2$ and p value, N = 539) and the grey shaded area indicates the 95% confidence interval.

## 4.4 Effect of photoacclimation on $a_{ph}^{*}(\lambda)$

The absorptive properties of phytoplankton are known to vary in the blue region of the spectrum due to changes in the relative proportion of non-photosynthetic or photoprotective pigments in the cells (Bricaud et al. 1995; Culver & Perry 1999). A non-photosynthetic pigment index (NPP), which may be considered as an index of phytoplankton photoacclimatory status, is the ratio of the concentration of non-photosynthetic pigments (the sum of zeaxanthin, diadinoxanthin, diatoxanthin, alloxanthin, β-carotene, and α-carotene) to total pigment concentration (i.e. chlorophylls, photosynthetic carotenoids, and non-photosynthetic carotenoids) (Babin et al. 1996). When NPP was plotted against TChl-*a* for surface samples, a negative relationship was observed (Figure 4.7). The Trades Biome showed markedly high NPP for the gyral SATL and NATR Provinces with considerable scatter, whereas, in general, provinces located within the Polar and Coastal Biomes had NPP values that were consistently low and less variable.

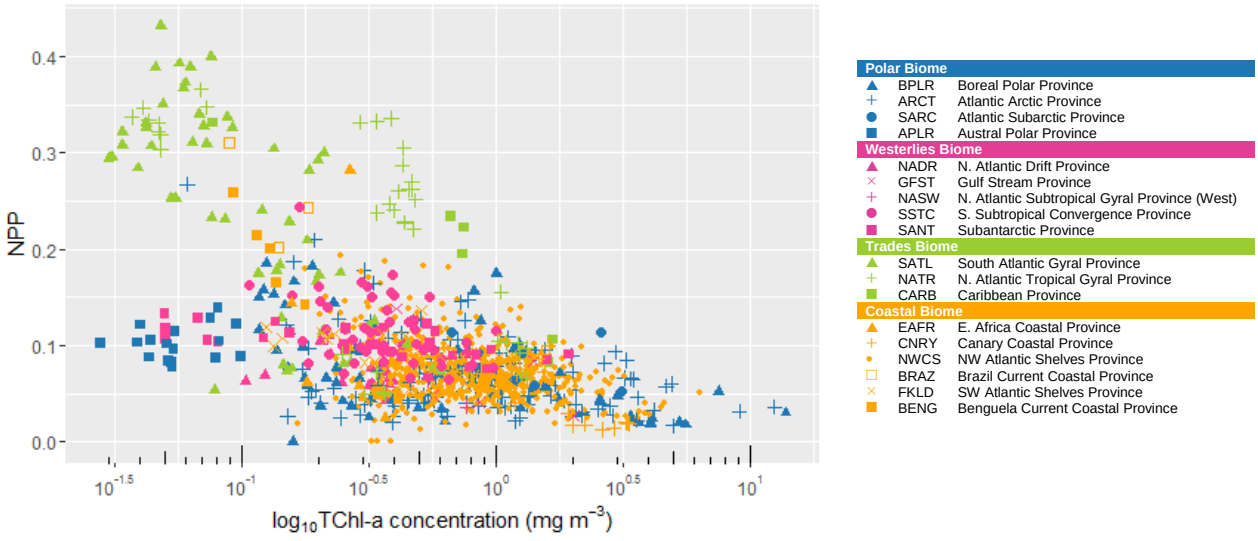



Figure 4.7: The non-photosynthetic pigment index (NPP) plotted against TChl-*a* for surface (0-20 m) samples.

Variations in NPP of phytoplankton populations in the surface mixed layer have been attributed to variations in light availability (Babin et al. 1996). The portion of solar irradiance over the spectral range of 400 to 700 nm which photosynthetic organisms can utilise to drive photosynthesis is defined as the photosynthetic available radiation or PAR (Falkowski & Raven 2007). To examine how changes in PAR affect NPP, we first plotted NPP against the daily PAR just below the surface, PAR($0^-$) (Figure 8*a*). Given *in situ* measurements of PAR($0^-$) were not available for many of the samples in the database, we used the R package '*phytotools*' (Silsbe & Malkin 2015) to estimate PAR($0^-$) values from the sampling date, geographic location, and atmospheric turbidity. The plot shows no significant correlation between PAR($0^-$) and NPP ($r^2 = 0.003$, $p = 0.16$).

Due to absorption and scattering by water and particles in the water, PAR decreases with depth. The rapidity of attenuation of PAR in the water column is characterised by the vertical attenuation coefficient for PAR, $K_d$, and is an important apparent optical property related to the turbidity of the water caused primarily by the presence of phytoplankton cells in the open ocean (Kirk 1994). In this study, when we plotted NPP against $K_d$, which was calculated from TChl-*a* using an empirical relationship derived by Morel & Maritorena (2001), we found that as $K_d$ values increased (the water became more turbid), there was a significant decrease in values of NPP ($\log_{10}$ NPP = -5.93 - 2.15$\log_{10} K_d$, $r^2 = 2.78$, $p < 0.05$) (Figure 8.2*b*).

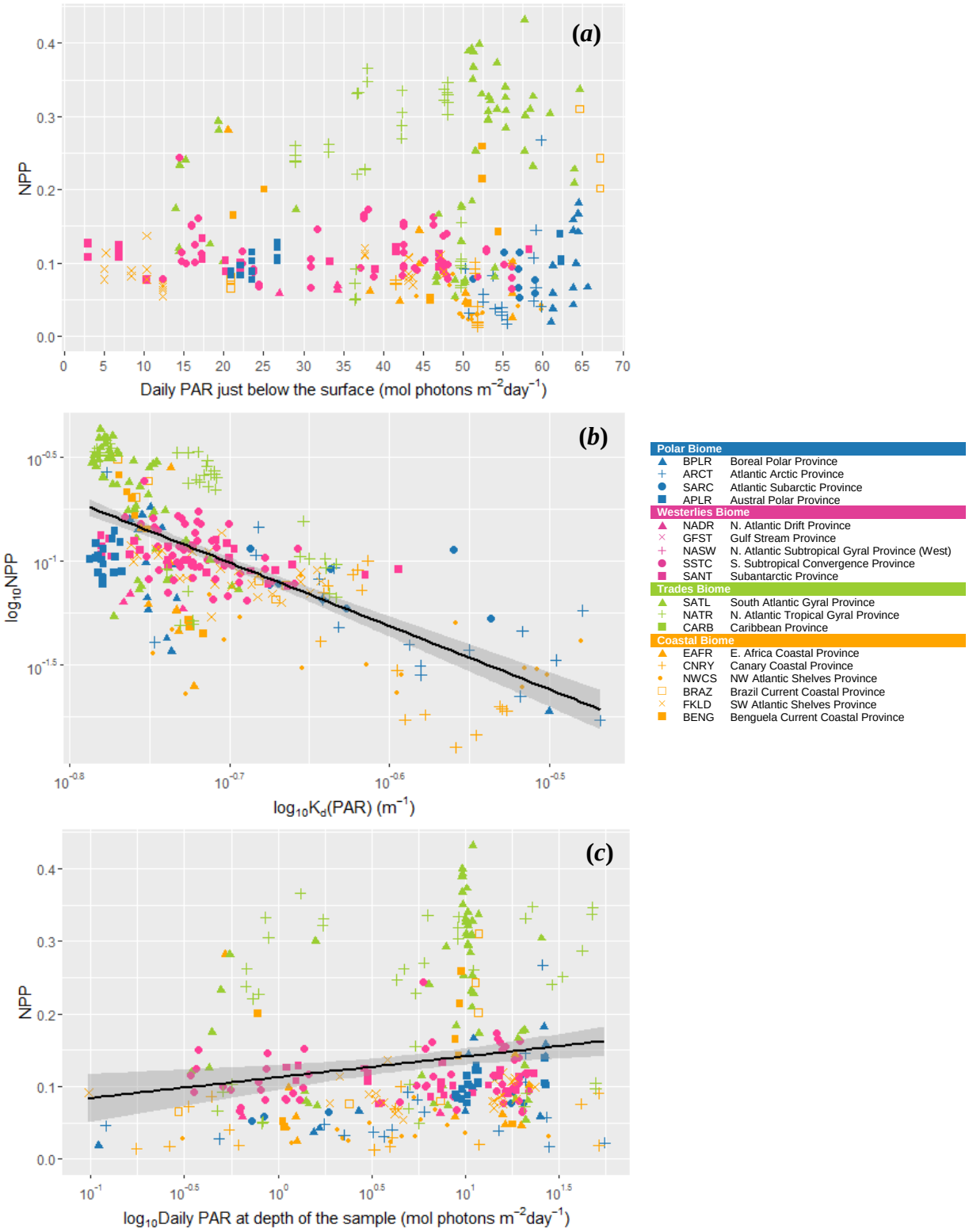



Figure 4.8: The non-photosynthetic pigment index (NPP) plotted against (*a*) the daily PAR just below the surface, PAR(0$^-$), (*b*) the vertical attenuation coefficient for PAR, $K_d$, for surface (0-20) samples, and (*c*) at depth of the sample, PAR(*z*).

Within the water column, PAR is attenuated in an exponential manner as a function of PAR($0^-$), $K_d$, and depth. Therefore, PAR at a given depth ($z$) of the sample, PAR($z$), can be computed as (Kirk 1994):

$$\mathrm{PAR}(z) = \mathrm{PAR}(0)\, e^{-K_d z}. \quad (4.1)$$

When values of NPP were plotted as a function of PAR($z$) (Figure 4.8*c*), a positive correlation was found ($\mathrm{NPP} = 0.113 + 0.03\log_{10}\mathrm{PAR}(z)$, $r^2 = 0.03$, $p < 0.05$). This positive correlation could be observed predominantly in the Polar Biome. The gyral SATL and NATR Provinces in the Trades Biome appeared to have markedly high values of NPP corresponding to high values of both PAR($0^-$) and PAR($z$).

To examine the effect of the relative abundance of non-photosynthetic pigments on $a^*_{ph}(\lambda)$, $a^*_{ph}(440)$ values were plotted against NPP (Figure 4.9). The plot shows a clear increase in $a^*_{ph}(440)$ with increasing NPP values, particularly for data collected in the Polar, Westerlies, and Coastal Biomes ($a^*_{ph}(440) = 0.16 + 0.071\log_{10}\mathrm{NPP}$, $r^2 = 0.20$, $p < 0.05$, $N = 690$). Note that the sample taken from the polar ARCT Province with an exceptionally high value of $a^*_{ph}(440)$ had the relatively high NPP values. The Trades Biome however showed significant scatter in the relationship between $a^*_{ph}(440)$ and NPP.

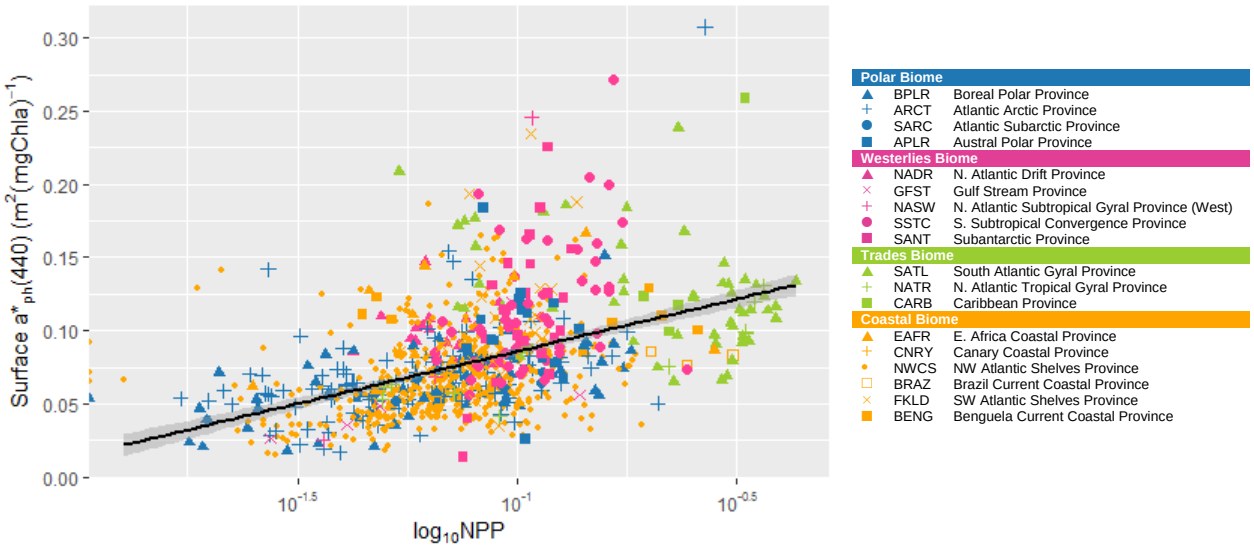



Figure 4.9: Chlorophyll-a specific absorption coefficients at 440 nm, $a^*_{ph}(440)$, plotted against the non-photosynthetic pigment index (NPP) for surface (0-20 m) samples.

## 4.5 Effect of phytoplankton community structure on $a^*_{ph}(\lambda)$

Although variability in $a^*_{ph}(\lambda)$ has been largely attributed to changes in pigment composition, especially the NPP, changes in cell size can be another source of variation in $a^*_{ph}(\lambda)$ (Kirk 1975; Bricaud et al. 2004). We first examined variation in the size composition of phytoplankton populations for the various oceanic biomes and provinces with respect to two remotely-sensed variables, temperature and TChl-*a*. We then assessed how variations in distribution of phytoplankton size structure were reflected in changes in $a^*_{ph}(\lambda)$.

Using equations 3.3 to 3.6, the percent contribution for each of the three pigment-based size classes (pico-, nano-, and microphytoplankton) to total phytoplankton biomass for samples collected within the top 20 m of the sea surface was calculated. The fractional contribution of the three size classes to total biomass for each sample is depicted using a ternary plot (Figure 4.10).

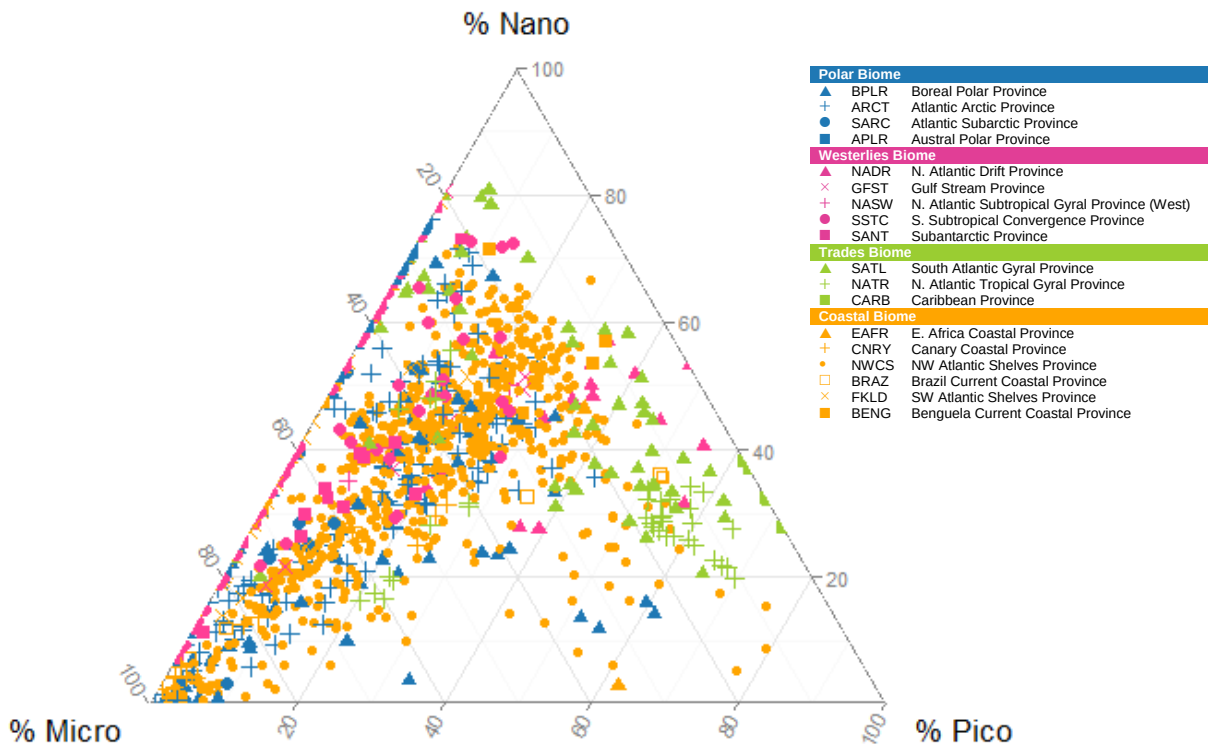



Figure 4.10: Ternary plot showing the percent contribution of each of the three pigment-based phytoplankton size classes to total phytoplankton biomass (percent pico, nano, and microphytoplankton) for surface (0-20 m) samples.

Microphytoplankton (20-200 µm) dominated the pigment biomass in the arctic and subarctic provinces, but were scarce in the gyral NATR and SATL Provinces and entirely absent from the CARB Province in the Trades Biome. Nanophytoplankton (2-20 µm) dominated (60 to 80%) in the Southern Ocean provinces APLR and SANT and tended to co-dominate with microphytoplankton in the Coastal and Westerlies Biomes. Picophytoplankton dominated (up to almost 80%) in the gyral and the CARB Province, but were completely absent in the APLR and the SANT.

When values of the percent contribution of each pigment-based size class to total phytoplankton biomass are plotted against temperature for surface samples, striking patterns are evident

(Figure 4.11*a*-*c*). $S_\mu$ tended to decrease with increasing temperature (Figure 4.11*a*), whereas $S_p$ (0.2-2 µm) showed the opposite pattern (Figure 4.11*c*). Although a majority of data collected in the Coastal Biome followed a negative correlation between temperature and $S_\mu$, several provinces in this biome, including the upwelling CNRY Province and part of the BRAZ Province, appeared to have abnormally high $S_\mu$ values at high temperature. There were two distinct trends in the relationship between temperature and $S_n$ (Figure 4.11*b*): a positive correlation was observed for data collected in the Coastal Biome, whereas a negative correlation was found in the Trades Biome over the temperature range of 12-26$^o$C. There appeared to be no relationship between temperature and the percent contribution of size classes for samples collected both in the Polar and the Westerlies Biomes, in which temperatures ranged from -2 to 12$^o$C

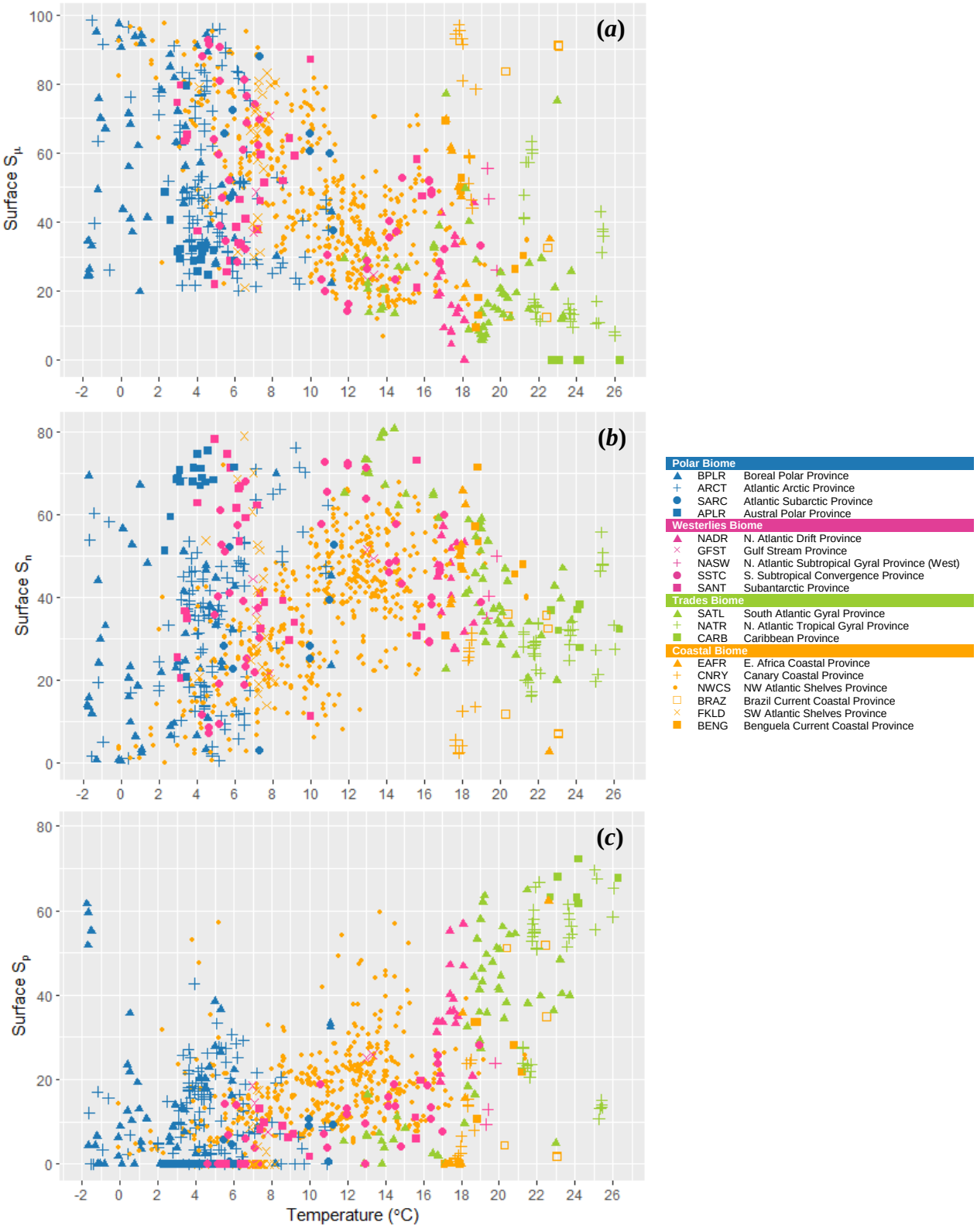



Figure 4.11: The percent contribution of (*a*) micro- ($S_\mu$), (*b*) nano- ($S_n$), and (*c*) picophytoplankton ($S_p$) plotted against temperature for surface (0-20 m) samples.




Figure 4.12: The percent contribution of (*a*) micro- ($S_\mu$), (*b*) nano- ($S_n$), and (*c*) picophyto-plankton ($S_n$) plotted against TChl-*a* for surface (0-20 m) samples.

The pigmented-based size classes were also plotted against TChl-*a* (Figure 4.12*a*-*c*), which is a remotely-sensed observable often used to infer the size structure of phytoplankton (Bricaud et al., 1995; Bouman et al., 2005). Data from all biomes showed a clear positive relationship between TChl-*a* and $S_\mu$ (Figure 4.12*a*), whereas $S_n$ and $S_p$ decreased with increasing TChl-*a* (Figure 4.12*b*, *c*).

To examine the relationship between phytoplankton size classes and the absorptive properties of phytoplankton, $a_{ph}^*(440)$ was plotted against the percent contribution of each size class to total Chl-*a* pigment (Figure 4.13*a*-*c*). There was a weak negative correlation between $S_\mu$ and values of $a_{ph}^*(440)$ ($a_{ph}^*(440) = 0.099 - 0.00045S_\mu$, $r^2 = 0.078$, $p < 0.05$, $N = 914$; Figure 4.13*a*). Conversely, $S_n$ tended to increase with an increase in $a_{ph}^*(440)$ values ($a_{ph}^*(440) = 0.094 + 0.00064S_n$, $r^2 = 0.094$, $p < 0.05$, $N = 914$; Figure 4.13*b*). There was no discernible relationship between $S_p$ and $a_{ph}^*(440)$ ($r^2 = 0.004$, $p \geq 0.05$, $N = 914$; Figure 4.13*c*).

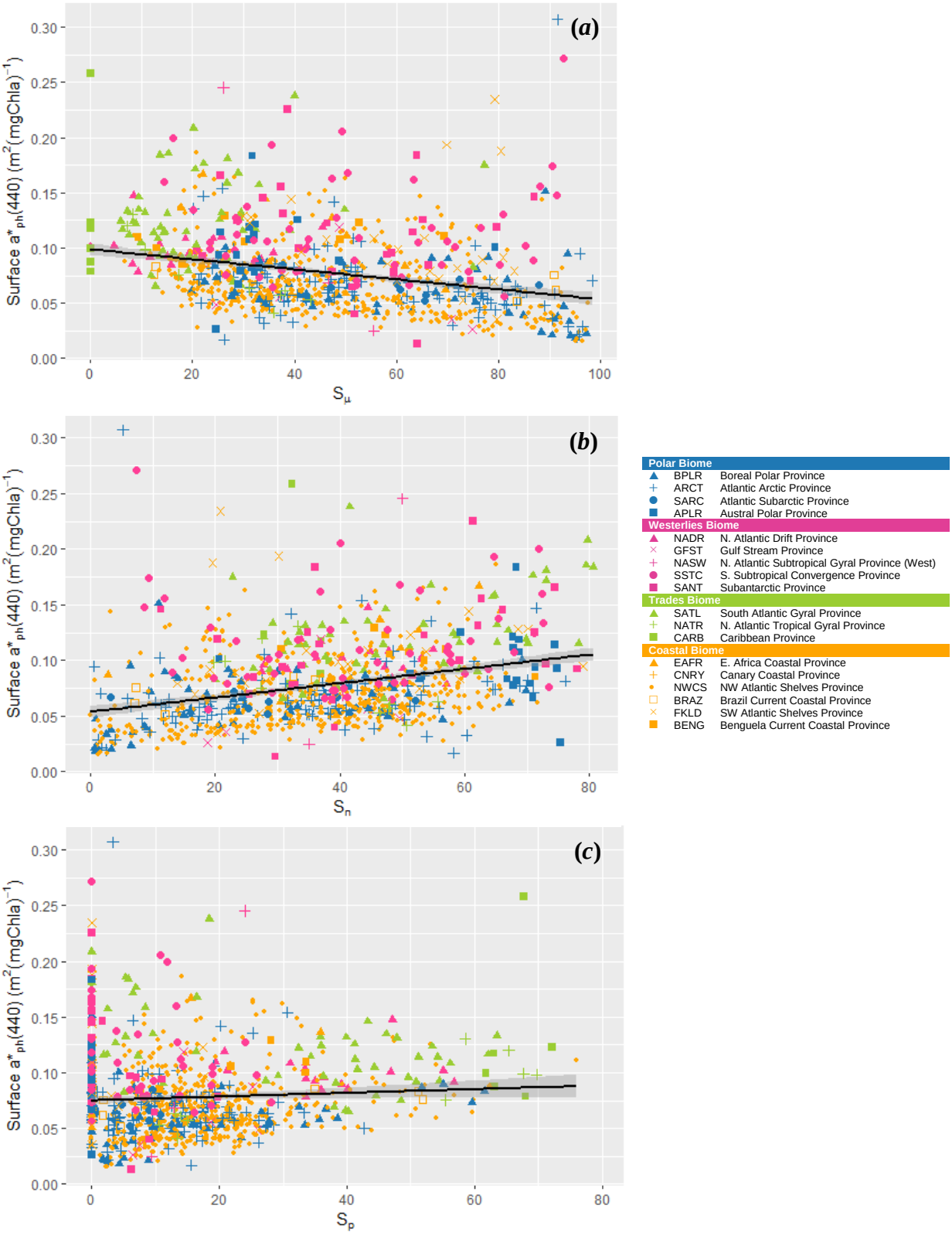



Figure 4.13: Chlorophyll *a*-specific absorption coefficients at 440 nm, $a^*_{ph}(440)$, plotted against the percent contribution of (*a*) micro- ($S_\mu$), (*b*) nano- ($S_n$), and (*c*) picophytoplankton ($S_n$).

When values of SI (equation 3.7) for the surface samples were plotted as a function of TChl-*a* (Figure 4.14), a positive correlation was observed with a high degree of scatter across the range of TChl-*a*, small picophytoplankton dominating in the oligotrophic gyral provinces and large microphytoplankton dominating in the eutrophic north polar waters. The Coastal and Westerlies Biomes contained a broad range of phytoplankton sizes and no clear relationship between size class and trophic status as index by TChl-*a* was observed.

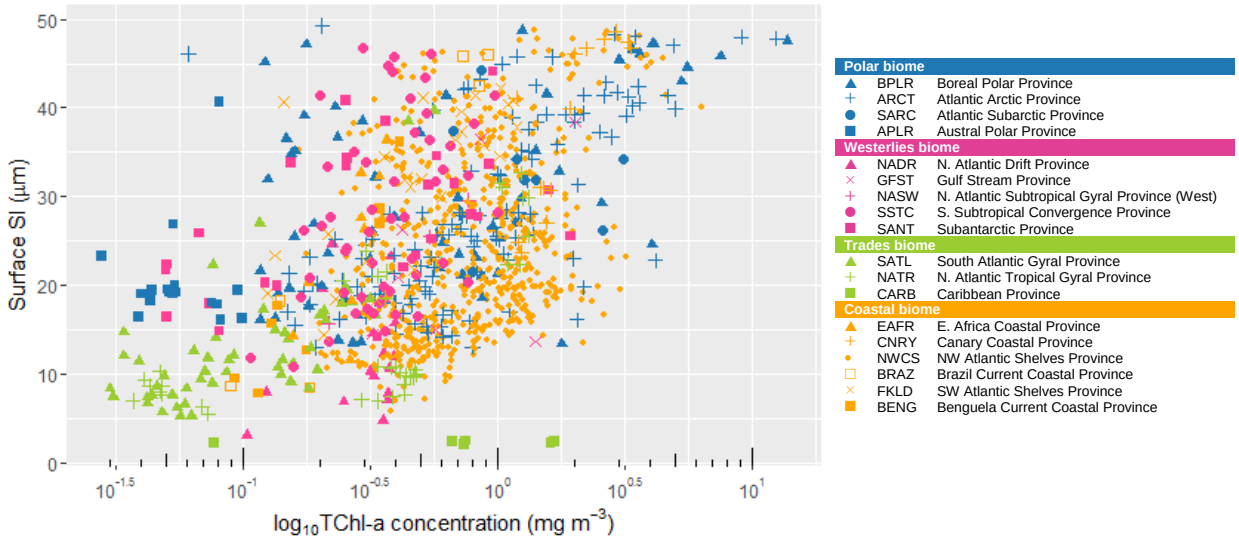



Figure 4.14: The size index (SI) plotted against TChl-*a* for the surface (0-20 m) samples.

To examine how cell size estimated using the SI relates to the absorptive properties of phytoplankton, we plotted $a^*_{ph}(440)$ against values of SI for surface samples (Figure 4.15). A weak negative correlation between the SI and $a^*_{ph}(440)$ was found ($a^*_{ph}(440)$ = 0.101 - 0.001*SI*, $r^2$ = 0.074, $p < 0.05$, N = 914).

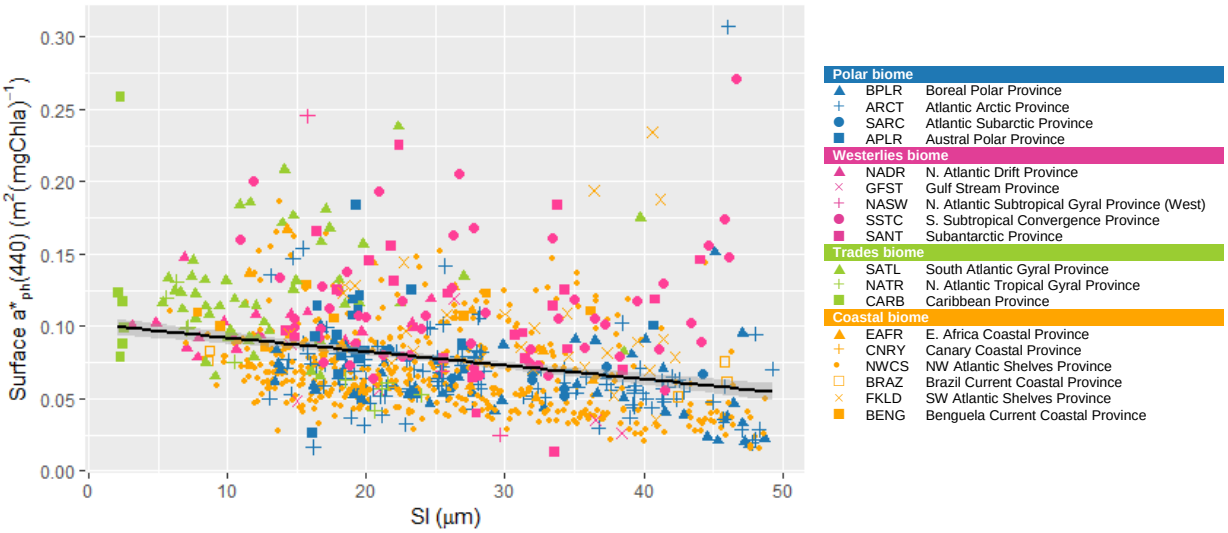



Figure 4.15: Chlorophyll *a*-specific absorption coefficients at 440 nm, $a^*_{ph}(440)$, plotted against values of SI for surface (0-20 m) samples.

# 5. Discussion

## 5.1 Effect of environmental factors on $a^*_{ph}(\lambda)$

Environmental variables known to modify the optical properties of phytoplankton include light history, temperature, and nutrient availability (Fujiki & Taguchi 2002; Stramski et al. 2002; Bouman et al. 2003; 2005; Platt et al. 2005). The data used in this study were confined to within the top 20 m of the water column, which limits the potential influence of vertical changes in light intensity on phytoplankton absorption. By restricting our dataset to the sea surface layer, the relationships derived from this dataset are rendered relevant to remote sensing applications, since ocean-color satellites are able to detect signal from only the first attenuation length of the water column (Gordon & McCluney 1975). Yet even within the top 20 m of the water column, light conditions may vary due to the latitudinal changes in incident irradiance, mixed-layer-depth dynamics, and turbidity, which in open ocean conditions is a function of TChl-*a*. Although direct measurements of irradiance were not available for many of the samples, seawater temperature and TChl-*a*, which may be considered proxies of degree of water column stratification and light attenuation, respectively, may be considered as indirect indicators of the factors governing underwater light conditions experienced by phytoplankton.

Seawater temperature is an environmental variable that provides information on the stability of the upper water-column in open ocean conditions and is routinely measured using both *in situ* and satellite-borne sensors. Sea-surface temperature has been identified as an ocean observable that is able to account for variability in the absorptive characteristics of marine phytoplankton that are caused by a combination of changes in the photoacclimatory status (pigment content) of cells or shifts in species composition, both of which have been shown to vary with water-

column stratification (Bouman et al. 2003). $a_{ph}^{*}(440)$ values increased with temperature (Figure 4.5), which is consistent with field observations in the Atlantic Ocean reported in Barlow et al. (2002) and Bouman et al. (2003). The geographical variability in $a_{ph}^{*}(440)$ reflects latitudinal changes in sea surface temperature and how surface temperature is related to vertical density gradients over a range of open ocean conditions. Broadly, surface light intensities and temperatures tend to increase from the poles to the equator. The combined effect of high incident irradiance and strongly stratified water column due to solar heating leads to high average light intensities within the surface mixed layer at low latitudes. Phytoplankton respond to elevated light intensities by decreasing their intracellular pigment concentration (Bidigare et al. 1990) and by increasing their relative concentrations of non-photosynthetic pigments (Fujiki & Taguchi 2002, section 5.2), both of which result in an increase in $a_{ph}^{*}(440)$. Conversely, in waters with low surface temperatures that are weakly stratified and hence more prone to surface mixing, cells will increase intracellular pigment concentrations as the average light in the mixed layer is reduced and thus have lower $a_{ph}^{*}(440)$ coefficients (Morel & Bricaud 1981; Stuart et al. 2000; Bouman et al. 2003). However, a significant degree of scatter in this positive correlation was observed, with the Trades and Polar Biomes exhibiting markedly different relationships between $a_{ph}^{*}(\lambda)$ and temperature. Possible reasons for a change in the relationship between temperature and phytoplankton absorptive properties for these specific oceanic biomes are discussed below.

The Trades Biome showed an inverse relationship between $a_{ph}^{*}(440)$ and temperature, with data from the North Atlantic gyres (NATR Province) having lower $a_{ph}^{*}(440)$ than those collected from the South Atlantic gyres (SATL Province). This may be due to the presence of

the colonial marine cyanobacterium *Trichodesmium* which has been reported to be abundant in the North Atlantic gyres but virtually absent from the South Atlantic gyres (Fernández et al. 2010). Aggregation of cells into larger colonies of *Trichodesmium* intensifies pigment packaging and thus results in a correspondingly reduced $a_{ph}^{*}(440)$. Although our study does not have direct evidence to implicate the presence of *Trichodesmium* as the main factor responsible for an observed decrease in light absorption efficiency in the NATR Province, we cannot rule out this factor as a potential cause.

In the Polar Biome, the lack of significant correlation between temperature and $a_{ph}^{*}(440)$ is likely a result of temperature's being a poor indicator of the physical properties of the water column. In this biome, temperature gradients are relatively small, when compared with those in temperate and low-latitude regions. A similar study in the southern Beaufort Sea (Matsuoka et al. 2009) also showed no clear relationship between $a_{ph}^{*}(443)$ and temperature. Although in the open ocean, temperature is a primary factor affecting the vertical density gradient and stratification of the water column, and thus regulating the supply of new nitrogen from the depth to the surface water (Bouman et al. 2003; Platt et al. 2005), in polar waters, where temperature is consistently low throughout the year, the effect of changes in seawater temperature on density and hence water-column stability is not as significant. Instead, the influx of freshwater from melting ice is a major contributor to salinity-driven stratification of the water column through the formation of a shallow and stable halocline (Matsuoka et al. 2009).

Thus the results presented here demonstrate that the relationship between temperature and $a_{ph}^{*}(\lambda)$ in the global ocean varies considerably across oceanographic regimes due to changes in

the relationship between temperature and other environmental drivers (either light or nutrients) that control phytoplankton community structure and photoacclimatory status. Thus, if sea-surface temperature is to be used to improve remote sensing algorithms, it must be done with consideration of the prevailing physical conditions. As Longhurst biomes are delineated based in part on the discontinuities of physical oceanographic processes and environmental variables such as irradiance (Longhurst 1998), it may be that SST-dependent algorithms should be invoked in a biome-specific or province-specific manner.

Another potential environmental source of variability in $a_{ph}^{*}(\lambda)$ examined in this study is ambient [$NO_2$+$NO_3$] as a proxy of nutrient availability. The relationship between $a_{ph}^{*}(\lambda)$ and macronutrient concentration has largely been attributed to changes in cell size over trophic gradients (Yentsch & Phinney 1989; Sosik & Mitchell 1995): regions with high rates of nutrient supply tend to be dominated by larger phytoplankton with low $a_{ph}^{*}(\lambda)$, and this inverse relationship between [$NO_2$+$NO_3$] and $a_{ph}^{*}(\lambda)$ has been documented in experimental and field studies of Barlow et al. (2002) and Stramski et al. (2002). However, in this study a weak positive relationship was found between [$NO_2$+$NO_3$] and $a_{ph}^{*}(440)$, with a large degree of scatter (Figure 4.6). One reason for the poor correlation could be that ambient nutrient levels may not be the best indicator of nutrient availability and that the vertical flux of nutrients into the photic zone may be a more appropriate measure of nutrient supply (Sosik 1996). For stations sampled within the high-nitrate, low-chlorophyll (HNLC) regions, mainly consisting of data collected from the SANT and the APLR Provinces, concentrations of surface [$NO_2$+$NO_3$] were consistently high and no apparent correlation between with [$NO_2$+$NO_3$] and $a_{ph}^{*}(440)$ was observed. It is well known that trace metal limitation of phytoplankton growth is common in

HNLC waters and experiments conducted on the Southern Ocean stations used in this study with high residual [$NO_2$+$NO_3$] showed clear evidence of iron stress (Browning et al. 2014). Since iron stress can induce changes in cellular concentration of Chl-*a* and other pigments, particularly the non-photosynthetic pigments, (Kosakowska et al. 2004), it is reasonable to assume that iron stress can also impact the absorptive properties of phytoplankton. Yet, studies on the direct effect of iron limitation on phytoplankton optical properties are still wanting.

In the subtropical gyral SATL Province, phytoplankton communities are normally dominated by prokaryotic picophytoplankton *Synechococcus* and *Prochlorococcus* (high-light and low-light ecotypes), and picoeukaryotes (Hickman et al. 2010; Bouman et al. 2011). Each of these groups of picophytoplankton has its own absorptive characteristics and distinctive pigment signature (see Figure 2 of Hickman et al. 2010). The depth distributions of these three picophytoplankton groups vary in relation to vertical gradients in temperature, nitrate, and light availability (Johnson et al. 2006; Hickman et al. 2010). Because this study selected only phytoplankton samples collected at the sea surface (< 20 m), [$NO_2$+$NO_3$] were chronically low, often falling below the limit of detection. Given that nutrient and optical measurements in oligotrophic waters often fall close to the limit of detection and that there were a limited number of samples from the gyral provinces, there remains a high degree of uncertainty as to the relationship between [$NO_2$+$NO_3$] and $a_{ph}^{*}(440)$ for the SATL Province.

Weak correlations between ambient [$NO_2$+$NO_3$] and $a_{ph}^{*}(\lambda)$, particularly when [$NO_2$+$NO_3$] values are low, have also been reported in the study of Bouman et al. (2003). The authors

challenged the validity of using ambient [$NO_2$+$NO_3$] as an indicator of nutrient availability and proposed that distance from the nitricline may be a more useful proxy (Sosik & Mitchell 1995).

## 5.2 Effect of non-photosynthetic pigments on $a^*_{ph}(\lambda)$

The results from this study clearly show that variations in the relative proportion of non-photosynthetic pigments (NPP) follow changes in TChl-*a*. NPP decreased from oligotrophic to eutrophic regions (Figure 4.7). In the tropical and subtropical gyral provinces, light intensities are normally high and the cyanobacterial picophytoplankton residing at the surface would acclimate to high light by decreasing the concentration of photosynthetic pigments relative to non-photosynthetic (photoprotective) pigments (Veldhuis & Kraay 2004). Johnsen & Sakshaug (1996) found that the concentrations of non-photosynthetic pigments (such as diadinoxanthin and diatoxanthin) relative to total pigment concentration in high-light acclimated diatoms and dinoflagellates can be up to 3 times higher when compared with those in low-light acclimated cells.

Zeaxanthin is a non-photosynthetic pigment that serves as a diagnostic pigment for the picocyanobacteria genera *Synechococcus* and *Prochlorococcus* (Vidussi et al. 2001; Uitz et al. 2006) and is abundant in the surface waters of the tropical and sub-tropical waters (Barlow et al. 2002; 2004; Bouman et al. 2003). In this study, zeaxanthin contributed significantly to the total concentration of non-photosynthetic pigment for samples collected from the gyral SATL (average = 52.83%) and NATR (74.23%) Provinces as well as from the Benguela Current Coastal (BENG) (33.17%) and the Brazil Current Coastal (BRAZ) (47.43%) Provinces. Barlow

et al. (2002) have also reported high relative concentrations of zeaxanthin in the surface waters of the Benguela upwelling ecosystem and along the Brazil-Falkland current.

Diadinoxanthin and alloxanthin were dominant non-photosynthetic pigments in the Arctic (the BPLR, ARCT, and SARC Provinces) and Antarctic (the APLR and SANT Provinces) samples. Alloxanthin indicates the presence of cryptophytes (Table 3.3), whereas diadinoxanthin is a ubiquitous pigment found in various phytoplankton taxa (Vidussi et al. 2001; Uitz et al. 2006). In one of the pigment samples from the ARCT Province an anomalously high NPP of 0.27 (Figure 4.7) was observed to correspond with the highest relative concentration of diadinoxanthin ([Diad]:[Total pigments] = 0.23). Variations in the relative abundance of diadinoxanthin in the Polar Biome have been associated with seasonal variations in incident solar irradiance and day length (Sakshaug & Slagstad 1991, Griffith et al. 2009).

In this study, photosynthetic available radiation just below the surface, PAR($0^-$), was not significantly correlated with changes in NPP (Figure 4.8*a*). This may due partly to uncertainty in PAR($0^-$) values using a clear-sky model provided in the R package '*phytotools*' (Silsbe & Malkin 2015), leading to a potential overestimation of PAR($0^-$) in many parts of the global oceans that are cloud-covered, in particular in temperate and polar oceans that have been reported to be consistently cloudy and receive a correspondingly reduced solar irradiance (Bishop & Rossow 1991; Kirk 1994). Another possible reason for the poor correlation between PAR($0^-$) and NPP could be that the intensity of the incident solar irradiance may not be a primary mechanism driving photoacclimation of phytoplankton and that the ambient light levels at depth

may be more important in inducing physiological response of phytoplankton (Cullen & Lewis 1988).

The underwater light availability of a given water body is largely influenced by turbidity which is an important determinant of vertical attenuation of light in that water body (Morel & Maritorena 2001). High $K_d$ values are commonly associated with eutrophic, turbid waters where particles in the water, such as phytoplankton, can lead to strong attenuation of light with depth. Conversely, clear, oligotrophic waters with low $K_d$ values (Kirk 1994), light penetrates much deeper. A strong negative correlation between $K_d$ and NPP observed in this study (Figure 4.8*b*) suggests that as the waters become less turbid as indicated by a decrease in values of $K_d$, a larger amount of PAR($0^-$) can penetrate the water column, inducing photoacclimatory response by phytoplankton through an increase in their NPP.

The extent to which variations in light availability influences the relative abundance of non-photosynthetic pigments and photoacclimatory status of phytoplankton becomes clearer when both $K_d$ and the intensity of PAR($0^-$) are used to estimate PAR($z$). The observed positive relationship between PAR($z$) and NPP (Figure 4.8*c*) illustrates that phytoplankton alter their intracellular NPP in responses to spatial and temporal variations in the underwater light environment. The weak correlation between PAR($z$) and NPP is likely caused by dynamic surface mixing in the water column (Falkowski 1983; Lewis et al. 1984; Cullen & Lewis 1988). By using PAR($z$), we are assuming that the water column is stable and phytoplankton residing at each depth would well acclimate to the ambient light level at that depth (Lewis et al. 1984). Yet, in the natural environment, phytoplankton cells are prone to vertical mixing that would

expose them to a range of light intensities within the surface mixed layer. As a result, they would acclimate to the average light in the mixed layer (Babin et al. 1996) rather than to the light level at any particular depth. Therefore, incorporating mixed layer depth into the calculation of the average light in the mixed layer would likely to improve the relationship between light availability and NPP and would be helpful in understanding how the physical dynamics of marine environments are reflected in the pigment composition of phytoplankton cells (Babin et al. 1996).

This large basin-scale dataset clearly shows that the absorptive properties of phytoplankton in the blue region of the spectrum are significantly affected by the relative proportion of non-photosynthetic pigments. As the relatively concentration of non-photosynthetic pigments increased, there was a corresponding increase in $a_{ph}^{*}(440)$ (Figure 4.9). This result is supported by several studies: Bricaud et al. (1995) for tropical and temperate waters in the North Atlantic, Sosik & Mitchell (1995) for the California Current System, Stuart et al. (2000) for the Labrador Sea, and Barlow et al. (2002) for the South Atlantic. The non-photosynthetic pigments diadinoxanthin and alloxanthin were major contributors to $a_{ph}^{*}(440)$ for data from Polar provinces, with the sample having the highest $a_{ph}^{*}(440)$ (0.31 $m^2$ (mg Chl-*a*)$^{-1}$) value having also the highest [Diad]:[Total pigments] ratio. The contribution of zeaxanthin to phytoplankton absorption in the blue region of the spectrum has also been demonstrated both in laboratory and field studies. In culture experiments on *Synechococcus* isolated from the Sargasso Sea, Moore et al. (1995) reported that zeaxanthin contributed significantly to $a_{ph}^{*}(\lambda)$ in the blue spectral range when the cells were exposed to high light intensities. In a study by Stuart et al. (1998) in

the Arabian Sea, zeaxanthin was found to account for up to 68% of variation in phytoplankton absorption at the 490 nm waveband.

It is clear from this and other field and culture studies that variations in $a^*_{ph}(\lambda)$ in the blue are strongly controlled by changes in NPP. Thus the effect of non-photosynthetic pigments on $a^*_{ph}(\lambda)$ should be taken into consideration when interpreting the remote sensing signal of sea-surface reflectance for various applications (chlorophyll retrieval algorithms), and in deriving quantum yields of photosynthesis (Babin et al. 1996) and fluorescence (Browning et al. 2014)

## 5.3 Distribution of size classes and its effect on $a^*_{ph}(\lambda)$

In this study pigment markers (Uitz et al. 2006) were used to quantify the percent contribution for the three phytoplankton size classes (pico-, nano-, and microphytoplankton) to total chlorophyll biomass. In addition, the size index (SI), proposed by Bricaud et al. (2004), was used to provide a gross estimate for the average cell diameter for a given phytoplankton sample. It is important to note that both of these approaches rely on concentrations of the same suite of diagnostic pigment markers, and hence any potential shortcomings or incorrect assumptions about how these pigment markers are related to phytoplankton size will lead to errors in both set of size-structure indices.

Previous studies have shown that the size structure of natural phytoplankton assemblages vary with changes in both TChl-*a* and temperature (Chisholm 1992; Ciotti et al. 2002; Bouman et al. 2003; Bricaud et al. 2004; Platt et al. 2005). In general, eutrophic (high chlorophyll) waters tend to be dominated by larger cells (microphytoplankton), whereas in oligotrophic (low

chlorophyll) waters smaller cells (picophytoplankton) are abundant (Chisholm 1992). In the open ocean, warm surface waters are typically more stratified, which leads to a surface depletion in nutrients (Platt et al. 2005). Nutrient limitation frequently leads to an increase in the relative abundance of small cells whose high surface-area-to-volume ratio allows them to outcompete larger cells under nutrient limited conditions (Barton et al. 2014). Conversely, cooling of surface waters favours surface mixing, allowing the entrainment of deep, nutrient-rich water to the surface, favouring the presence of large cells in the upper water column.

The relationship between the percent contribution to total pigment biomass for each size class and two remotely sensed observables used in phytoplankton biogeography studies (temperature and TChl-*a*) were examined. Correlations differed between biogeochemical provinces (Figures 4.11-4.12). In the provinces located within the Trades Biome (SATL and NATR) there was a dominance of picophytoplankton in the warm, highly-stratified surface waters (Figure 4.11*c* and 4.12*c*) and $S_\mu$ was correspondingly low (Figure 4.11*a* and 4.12*a*) which is consistent with the findings of several studies of subtropical, open-ocean ecosystems (Barlow et al. 2002; Bricaud et al. 2004). In the eastern SATL Province (0-10˚E), markedly high $S_n$ (> 60%) was observed in the surface waters with temperature ranging between 11 and 17˚C (Figure 4.11*b*). This is consistent with the recent study of Estrada et al. (2016) who found an elevated number of coccolithophores and unidentified nanoflagellates within the top 3 m of the surface waters at similar latitudes within the SATL Province. No clear pattern between phytoplankton size structure and environmental variables was observed in the CARB Province, however this was due in part to the low number of surface pigment samples (N=6) collected from the eastern Gulf of Mexico (Figure 3.1). These 6 samples all showed a dominance of picophytoplankton at high

temperature. Several studies have reported a high abundance of picophytoplankton in different regions of the Gulf of Mexico relative to larger phytoplankton (Okolodkov 2003; Wawrik et al. 2003; Linacre et al. 2015), and these picophytoplantkon tend to be associated with the intrusion of the warm Loop Current (Longhurst 1998) into the Gulf of Mexico (see also Linacre et al. 2015).

Micro- and nanophytoplankton co-dominated in the surface waters of the Polar Biome. In the Atlantic Arctic (BPLR, ARCT, and SARC Provinces), diatoms, coccolithophores, and the haptophyte *Phaeocystis* spp. are frequently abundant and can form large blooms (Harrison & Cota 1991; Longhurst 1998; Le Moigne et al. 2015). In the Antarctic APLR Province (Polar Biome) and the SANT Province (Westerlies Biome) of the Southern Ocean, the high (> 65%) percent contribution for nanophytoplankton, indicated by high concentrations of 19′-Hex and 19′-But, was observed which indicates the presence of prymnesiophytes (Figures 4.11*b* and 4.12*b*) and is consistent with the findings of Uitz et al. (2006). Temperature was not a good predictor of phytoplankton community structure in the Polar Biome, probably because temperature is often not the dominant factor governing the physical structure of the water column. Instead, the freeze-melt cycle of sea ice causes salinity-driven water-column stratification (Harrison & Cota 1991; Longhurst 1998; Dierssen et al. 2002), which occurs within a narrow temperature range. Community structure within the Westerlies Biome is strongly associated with water-column stratification (Longhurst 1998). As surface warming increases and wind stress weakens, the water column becomes more straitified leading to a shift from large to small cells. This is illustrated in Figure 4.11 where the percent contribution for

microphytoplankton decreased and that for picophytoplankton increased with increasing surface temperature.

The Coastal Biome is hydrodynamically complex with high topographical diversity and covers a large latitudinal range (Longhurst 1998). The majority of the data collected in this biome belongs to the NWCS Province. This temperate North Atlantic province has large cells dominating in cold, high TChl-*a* waters and smaller cells preferring the warm waters with low TChl-*a* (Figures 4.11-4.12). A dominance of larger cells in the FKLD Province may be explained by strong winter mixing and the presence of the Falkland Current, which carries the cold, macronutrient-rich waters from the subantarctic region (Longhurst 1998). For the upwelling coastal provinces (EAFR, CNRY, BRAZ, and BENG) none of the pigment-based size classes showed a strong relationship with temperature. However, when the percent size classes for these provinces were plotted against TChl-*a* (Figure 4.12), clear patterns emerged: moving from more oligotrophic to more eutrophic waters, $S_\mu$ increased, whereas $S_n$ and $S_p$ decreased. An increase in the average cell size of phytoplankton with increasing TChl-*a* associated with upwelling zones has also been reported in Bricaud et al. (2004). Thus TChl-*a* is a more reliable indicator of phytoplankton size classes in these upwelling provinces, possibly due to the poor relationship between temperature and nutrient supply for these oceanic regimes.

The relationship between $a_{ph}^*(440)$ and phytoplankton cell size (SI) obtained in this study was not as strong as anticipated (Figure 4.15). Previous theoretical, experimental, and field studies have demonstrated that larger cells tend to have reduced $a_{ph}^*(\lambda)$ (Duyens 1956; Kirk 1975; Geider & Osborne 1987; Morel & Bricaud 1981; Bricaud et al. 1995). Data from the SSTC and

SANT Provinces, which are considered HNLC regions, showed relatively high values of $a_{ph}^{*}(440)$ coinciding with larger cell sizes. In the HNLC areas, phytoplankton are typically dominated by prymnesiophytes (Bouman et al. 2012) which are classified using pigment markers (19′-Hex and 19′-But) as belonging to the nanophytoplankton size class. However, molecular data suggest that it is actually small, non-calcifying prymnesiophytes that contribute significantly to phytoplankton pigment biomass (Liu et al. 2009), and in the Atlantic Ocean, prymnesiophytes have been found to fall within the picophytoplankton size range (Cuvelier et al. 2010). Thus the allocation of samples from the SSTC and SANT Provinces into certain size classes based on pigment markers may be prone to error. Instead, samples with pigments associated with prymnesiophytes may represent cells less than 2-3 μm in diameter, which would explain the higher light absorption efficiencies. This suggests that a different set of pigment indices need to be derived for these HNLC waters to relate phytoplankton size structure to pigment markers.

Diagnostic pigments offer us a potential tool for classifying samples into size or taxonomic groups based on their pigment composition. Unlike some conventional methods which often fail to detect very small picophytoplankton (light microscopy) or very large microphytoplankton (flow cytometry), pigment markers can be used in estimating the size of phytoplankton over the entire size range (Claustre 1994). Nevertheless, chemotaxonomic approaches suffer several limitations. Some diagnostic pigments are shared amongst more than one phytoplankton group. For instance, fucoxanthin which is a marker pigment for diatoms (microphytoplankton) can also be found in prymnesiophytes (nanophytoplankton) (Ras et al. 2008). Moreover, members of a particular phytoplankton taxonomic group can fall into different size classes. For example,

diatoms are typically classified into the microphytoplankton but can sometimes be found in the nano-size range (Uitz et al. 2009). In addition, although zeaxanthin and divinyl-chlorophyll *b* are typically used to estimate the abundance of prokaryotic picophytoplankton, they do not account for a diverse community of picoeukaryotes, which have been increasingly recognized as abundant primary producers using molecular techniques (Cuvelier et al. 2010; Bouman et al. 2011; Massana 2011; Aquino-Cruz et al. 2013).

# 6. Conclusions and future work

Pigment and absorption data collected from surface waters across the Atlantic Basin were used to examine potential factors governing the size structure and absorptive properties of natural phytoplankton communities. By dividing a large dataset into different biogeochemical biomes and provinces (Longhurst 1998), the impact of environmental factors on both phytoplankton community structure and absorption efficiency was examined over regional to basin scales.

Temperature was shown to be a predictor of phytoplankton size structure in the tropical and subtropical gyral provinces, yet could not explain shifts in phytoplankton size structure in the Polar Biomes. In sub-Arctic and sub-Antarctic regions, water-column stratification is largely driven by changes in salinity as a result of the freeze-melt cycle of sea ice (Harrison & Cota 1991; Dierssen et al. 2002). Thus, the use of satellite-based salinity should be explored as a tool for examining variations in the size structure of phytoplankton at high latitudes.

Nutrient availability represented in this study as ambient surface [$NO_2$+$NO_3$] was shown to have a weak positive correlation with $a_{ph}^{*}(440)$, with a considerable degree of scatter. This pattern differed from the results obtained in previous experimental and field studies (Barlow et al. 2002; Stramski et al. 2002). Temperature also showed a weak correlation with $a_{ph}^{*}(440)$. However, when each oceanic biome was examined separately, the relationships between temperature and phytoplankton absorption efficiency varied depending on how different environmental factors (e.g. light or nutrient availability) that are known to control phytoplankton community structure and photoacclimatory status varied with respect to surface temperature. Further work on developing a mechanistic understanding of how environmental factors govern phytoplankton

absorptive properties through multifactorial bioassays (light, temperature, nutrients) on cultured and natural populations is required if ocean observables (chlorophyll and temperature) are to be used in satellite-based studies of phytoplankton macroecology.

The chlorophyll *a*-specific absorption coefficient of the phytoplankton at 440 nm, $a_{ph}^{*}(440)$, was shown to be significantly influenced by the relative proportions of non-photosynthetic pigments, which in turn was inversely correlated with TChl-*a*. The effect of non-photosynthetic pigments on phytoplankton absorption efficiency has been observed in other studies in different regions of the Atlantic Basin (Bricaud et al. 1995; Lazzara et al. 1996; Stuart et al. 2000; Barlow et al. 2002). Our study did not show strong correlation between $a_{ph}^{*}(440)$ and pigment indices of phytoplankton size, although there was a general tendency for larger cells to exhibit lower $a_{ph}^{*}(440)$.

It is clear from these results that the relative concentration of non-photosynthetic pigments accounted for a significant fraction of the variability in $a_{ph}^{*}(440)$ and that the relationships between pigment indices for the various phytoplankton size classes were much more variable. Another area for future study is to develop a quantitative understanding of the relative roles cell size, pigment composition and the package effect have in governing the absorptive properties of cell. Although theoretical models do exist, datasets to validate these models are rare, especially for natural phytoplankton assemblages. One way of quantifying the package effect is through examining the specific absorption coefficient at the red absorption peak of phytoplankton (676 nm). Absorption at the red peak is largely caused by chlorophyll a and its derivatives, making the effect of other accessory pigments on variations in $a_{ph}^{*}(676)$ negligible

(Bouman et al. 2003; Platt et al. 2005). Yet to fully disentangle the effect of cell size versus pigment content on pigment packaging, detailed measurements on the size spectra of natural assemblages will be required, which are lacking in many bio-optical datasets.

# References


Acevedo-Trejos, E. et al., 2015. Mechanisms shaping size structure and functional diversity of phytoplankton communities in the ocean. *Scientific Reports*, 5, p.8918.

Agusti, S. et al., 2015. Ubiquitous healthy diatoms in the deep sea confirm deep carbon injection by the biological pump. *Nature Communications*, 6, p.7608.

Aquino-Cruz, A. et al., 2013. Studies on picophytoplankton in the southern Gulf of Mexico: recognition of picoprokaryotes and abundances of picophytoplankton during dry season. *Brazilian Journal of Oceanography*, 61(4), pp.265–276.

Babin, M. et al., 1996. Nitrogen- and irradiance-dependent variations of the maximum quantum yield of carbon fixation in eutrophic, mesotrophic and oligotrophic marine systems. *Deep-Sea Research Part I*, 43(8), pp.1241–1272.

Barlow, R.G. et al., 2002. Phytoplankton pigment and absorption characteristics along meridional transects in the Atlantic Ocean. *Deep-Sea Research Part I: Oceanographic Research Papers*, 49(4), pp.637–660.

Barlow, R.G. et al., 2004. Pigment adaptations in surface phytoplankton along the eastern boundary of the Atlantic Ocean. *Marine Ecology Progress Series*, 281, pp.13–26.

Barlow, R.G., Cummings, D.G. & Gibb, S.W., 1997. Improved resolution of mono- and divinyl chlorophylls a and b and zeaxanthin and lutein in phytoplankton extracts using reverse phase C-8 HPLC. *Marine Ecology Progress Series*, 161, pp.303–307.

Barton, A.D. et al., 2014. The impact of fine-scale turbulence on phytoplankton community structure. *Limnology & Oceanography: Fluids & Environments*, 4(APRIL), pp.34–49.

Bidigare, R.R., 2013. Analysis of algal chlorophylls and carotenoids. In D. C. Hurd & D. W. Spencer, eds. *Marine Particles: Analysis and Characterization*. American Geophysical Union, pp. 119–123.

Bidigare, R.R., 2005. High-performance liquid chromatography determination of algal chlorophylls and their degradation products. In *Standard Methods for the Examination of Water and Wastewater, Section 10200 H.4*. Washington, D. C.: American Public Health Association, pp. 10–23.

Bidigare, R.R. et al., 1990. In vivo absorption properties of algal pigments. *SPIE Proceedings 1302, Ocean Optics X*, 290.

Bidigare, R.R., Van Heukelem, L. & Trees, C.., 2005. Analysis of algal pigments by high-performance liquid chromatography. In R. A. Andersen, ed. *Algal Culturing Techniques*. New York, USA: Academic Press, pp. 432–435.

Biller, S.J. et al., 2014. Prochlorococcus: the structure and function of collective diversity. *Nature Reviews Microbiology*, 13(1), pp.13–27.

Billington, N., 1991. A comparison of three methods of measuring phytoplankton biomass on a daily and seasonal basis. *Hydrobiologia*, 226(1), pp.1–15.

Bishop, J.K.B. & Rossow, W.B., 1991. Spatial and temporal variability of global surface solar irradiance. *Journal of Geophysical Research*, 96(C9), pp.16839–16858.

Bouman, H.A. et al., 2000. Bio-optical properties of the subtropical North Atlantic. I. Vertical variability. *Marine Ecology Progress Series*, 200, pp.3–18.

Bouman, H.A. et al., 2005. Dependence of light-saturated photosynthesis on temperature and community structure. *Deep-Sea Research Part I: Oceanographic Research Papers*, 52(7), pp.1284–1299.

Bouman, H.A. et al., 2012. Phytoplankton community structure in a high-nutrient, low-chlorophyll region of the eastern Pacific Subantarctic region during winter-mixed and summer-stratified conditions. *Deep-Sea Research Part I: Oceanographic Research Papers*, 69, pp.1–11.

Bouman, H.A. et al., 2003. Temperature as indicator of optical properties and community structure of marine phytoplankton: Implications for remote sensing. *Marine Ecology Progress Series*, 258, pp.19–30.

Bouman, H.A. et al., 2011. Water-column stratification governs the community structure of subtropical marine picophytoplankton. *Environmental Microbiology Reports*, 3(4), pp.473–482.

Brewin, R.J.W. et al., 2011. Model of phytoplankton absorption based on three size classes. *Applied Optics*, 50(22), pp.4535–4549.

Bricaud, A. et al., 2004. Natural variability of phytoplanktonic absorption in oceanic waters: Influence of the size structure of algal populations. *Journal of Geophysical Research: Oceans*, 109(11), pp.1–12.

Bricaud, A. et al., 1995. Variability in the chlorophyll-specific absorption coefficients of natural phytoplankton: analysis and parameterization. *Journal of Geophysical Research*, 100, pp.13321–13332.

Bricaud, A. & Stramski, D., 1990. Spectral absorption coefficients of living phytoplankton and nonalgal biogenous matter: a comparison between the Peru upwelling area and the Sargasso Sea. *Limnology and Oceanography*, 35(3), pp.562–582.

Browning, T.J., Bouman, H.A. & Moore, M.C., 2014. Satellite-detected fluorescence: decouplingnonphotochemical quenching from ironstress signals in the South Atlantic and Southern Ocean. *Global Biogeochemical Cycles*, 28, pp.510–524.

Caruana, A.M.N. & Malin, G., 2014. The variability in DMSP content and DMSP lyase activity in marine dinoflagellates. *Progress in Oceanography*, 120, pp.410–424.

Charlson, R.J. et al., 1987. Oceanic phytoplankton, atmospheric sulphur, cloud albedo and climate. *Nature*, 326, pp.655–661.

Chisholm, S.W., 1992. Phytoplankton size. In P. G. Falkoski & A. D. Woodhead, eds. *Primary Productivity and Biogeochemical Cycles in the Sea*. New York, USA: Plenum Press, pp. 213–237.

Ciotti, A.M., Lewis, M.R. & Cullen, J.J., 2002. Assessment of the relationships between dominant cell size in natural phytoplankton communities and the spectral shape of the absorption coefficient. *Limnology and Oceanography*, 47(2), pp.404–417.

Claustre, H., 1994. The trophic status of various oceanic provinces as revealed by phytoplankton pigment signatures. *Limnology and Oceanography*, 39(5), pp.1206–1210.

Claustre, H. & Marty, J.-C., 1995. Specific phytoplankton biomasses and their relation to primary production in the tropical North Atlantic. *Deep Sea Research Part I: Oceanographic Research Papers*, 42(8), pp.1475–1493.

Cleveland, J.S. & Weidemann, A.D., 1993. Quantifying absorption by aquatic particles: A multiple scattering correction for glass-fiber filters. *Limnology and Oceanography*, 38, pp.1321–1327.

Cullen, J.J. et al., 1997. Optical detection and assessment of algal blooms. *Limnology and Oceanography*, 42, pp.1223–1239.

Cullen, J.J. & Lewis, M.R., 1988. The kinetics of algal adaptation in the context of vertical mixing. *Journal of Plankton Research*, 10(5), pp.1039–1063.

Culver, M.E. & Perry, M.J., 1999. The response of photosynthetic absorption coefficients to irradiance in culture and in tidally mixed estuarine waters. *Limnology and Oceanography*, 44(1), pp.24–36.

Cuvelier, M.L. et al., 2010. Targeted metagenomics and ecology of globally important uncultured eukaryotic phytoplankton. *PNAS*, 107, pp.14679–14684.

Dierssen, H.M., Smith, R.C. & Vernet, M., 2002. Glacial meltwater dynamics in coastal waters west of the Antarctic peninsula. *PNAS*, 99, pp.1790–1795.

Duyens, L.N.M., 1956. The flattering of the absorption spectrum of suspensions, as compared to that of solutions. *Biochimica et Biophysica Acta*, 19, pp.1–12.

Estrada, M. et al., 2016. Phytoplankton across Tropical and Subtropical Regions of the Atlantic, Indian and Pacific Oceans. *PLOS ONE*, 11(3).

Falkowski, P.G., 1983. Light-shade adaptation and vertical mixing of marine phytoplankton: a comparative field study. *Journal of Marine Research*, 41, pp.215–237.

Falkowski, P.G., 1994. The role of phytoplankton photosynthesis in global biogeochemical cycles. *Photosynthesis Research*, 39(3), pp.235–258.

Falkowski, P.G. & Raven, J.A., 2007. *Aquatic Photosynthesis* 2nd ed., Princeton University Press.

Fernández, A. et al., 2010. Latitudinal distribution of Trichodesmium spp. and N2 fixation in the Atlantic Ocean. *Biogeosciences*, 7, pp.3167–3176.

Field, C.B., 1998. Primary production of the biosphere: integrating terrestrial and oceanic components. *Science*, 281(5374), pp.237–240.

Finkel, Z. V. et al., 2010. Phytoplankton in a changing world: cell size and elemental stoichiometry. *Journal of Plankton Research*, 32(1), pp.119–137.

Flombaum, P. et al., 2013. Present and future global distributions of the marine Cyanobacteria Prochlrococcus and Synechococcus. *PNAS*, 110(24), pp.9824–9829.

Fujiki, T. & Taguchi, S., 2002. Variability in chlorophyll a specific absorption coefficient in marine phytoplankton as a function of cell size and irradiance. *Journal of Plankton Research*, 24, pp.859–874.

Garrido, J.L. et al., 2011. New HPLC separation techniques. In S. Roy et al., eds. *Phytoplankton Pigments: Characterization, Chemotaxonomy and Application in Oceanography*. Cambridge, UK: Cambridge University Press, pp. 165–194.

Geider, R.J. & Osborne, B.A., 1987. Light absorption by a marine diatom: experimental observations and theoretical calculations of the package effect in a small Thalassiosira species. *Marine Biology*, 96(2), pp.299–308.

Gibb, S.. et al., 2000. Surface phytoplankton pigment distributions in the Atlantic Ocean: an assessment of basin scale variability between 50°N and 50°S. *Progress in Oceanography*, 45(3-4), pp.339–368.

Gordon, H.R. & McCluney, W.R., 1975. Estimation of the depth of sunlight penetration in the sea for remote sensing. *Applied optics*, 14(2), pp.413–6.

Griffith, G.P., Vennell, R. & Lamare, M.D., 2009. Diadinoxanthin cycle of the bottom ice algal community during spring in McMurdo Sound, Antarctica. *Polar Biology*, 32(4), pp.623–636.

Hammer, A.C. & Pitchford, J.W., 2005. The role of mixotrophy in plankton bloom dynamics, and the consequences for productivity. *ICES Journal of Marine Science*, 62(5), pp.833–840.

Harrison, W.G. & Cota, G.F., 1991. Primary production in polar waters: relation to nutrient availability. *Polar Research*, 10(1), pp.87–104.

Head, E.J.H. & Horne, E.P.W., 1993. Pigment transformation and vertical flux in an area of convergence in the North Atlantic. *Deep Sea Research Part II: Topical Studies in Oceanography*, 40(1-2), pp.329–346.

Hickman, A.E. et al., 2010. Modelling the effects of chromatic adaptation on phytoplankton community structure in the oligotrophic ocean. *Marine Ecology Progress Series*, 406, pp.1–17.

Higgins, H.W., Wright, S.W. & Schluter, L., 2011. Quantitative interpretation of chemo-taxonomic pigment data. In S. Roy et al., eds. *Phytoplankton Pigments: Characterization, Chemotaxonomy and Application in Oceanography*. Cambridge, UK: Cambridge University Press, pp. 257–313.

Hoepffner, N. & Sathyendranath, S., 1992. Bio-optical characteristics of coastal waters: Absorption spectra of phytoplankton and pigment distribution in the western North Atlantic. *Limnology and Oceanography*, 37(8), pp.1660–1679.

Hoepffner, N. & Sathyendranath, S., 1991. Effect of pigment composition on absorption properties of phytoplankton. *Marine Ecology Progress Series*, 73, pp.11–23.

Holm-Hansen, O. et al., 1965. Fluorometric Determination of Chlorophyll. *ICES Journal of Marine Science*, 30(1), pp.3–15.

IOCCG, 2014. *Phytoplankton functional types from space* S. Sathyendranath, ed., Dartmouth, Canada.

IOCCG, 2006. *Remote Sensing of Inherent Optical Properties: Fundamentals, Tests of Algorithms, and Applications* Z. Lee, ed., Dartmouth, Canada.

Jackson, T., 2013. *Phytoplankton Community Structure, Photophysiology and Primary Production in the Atlantic Arctic*. University of Oxford.

Jeffrey, S.W. & Mantoura, R.F.C., 1997. Development of pigment methods for oceanography: SCOR-supported Working Groups and objectives. In S. W. Jeffrey, R. F. C. Mantoura, & S. W. Wright, eds. *Phytoplankton Pigments in Oceanography: Guidelines to Modern Methods*. Paris, France, pp. 19–36.

Jeffrey, S.W. & Vesk, M., 1997. Introduction to marine phytoplankton and their pigment signatures. In S. W. Jeffrey, R. F. C. Mantoura, & S. W. Wright, eds. *Phytoplankton pigments in oceanography: guidelines to modern methods*. Paris, France: UNESCO Publishing, pp. 37–84.

Jeffrey, S.W., Wright, S.W. & Zapata, M., 2011. Microalgal classes and their signature pigments. In S. Roy et al., eds. *Phytoplankton Pigments: Characterization, Chemotaxonomy and Application in Oceanography*. Cambridge, UK: Cambridge University Press, pp. 3–45.

Johnsen, G. et al., 2011. In vivo bio-optical properties of phytoplankton pigments. In S. Roy et al., eds. *Phytoplankton Pigments: Characterization, Chemotaxonomy and Application in Oceanography*. Cambridge, UK: Cambridge University Press, pp. 496–537.

Johnsen, G. & Sakshaug, E., 1996. Light harvesting in bloom-forming marine phytoplankton: species-specificity and photoacclimation. *Scientia Marina*, 60, pp.47–56.

Johnson, Z.I. et al., 2006. Partitioning among Prochlorococcus ecotypes along environmental gradients. *Science*, 311, pp.1737–1740.

Johnson, Z.I. & Lin, Y., 2009. Prochlorococcus: approved for export. *Proceedings of the National Academy of Sciences of the United States of America*, 106(26), pp.10400–10401.

Keller, M.D., 1989. Dimethyl sulfide production and marine phytoplankton: the importance of species composition and cell size. *Biological Oceanography*, 6(5-6), pp.375–382.

Kirk, J.T.O., 1975. A theoretical analysis of the contribution of algal cells to the attenuation of light within natural waters I. General treatment of suspensions of pigmented cells. *New Phytologist*, 75(1), pp.11–20.

Kirk, J.T.O., 1976. A theoretical analysis of the contribution of algal cells to the attenuation of light within natural waters. III. Cylindrical and spheroidal cells. *New Phytologist*, 77, pp.341–358.

Kirk, J.T.O., 1994. *Light and Photosynthesis in Aquatic Ecosystems*, Cambridge, UK: Cambridge University Press.

Kishino, M. et al., 1985. Estimation of the spectral absorption coefficients of phytoplankton in the sea. *Bulletin of Marine Science*, 37(2), pp.634–642.

Kosakowska, A. et al., 2004. Qualitative and quantitative composition of pigments in Phaeodactylum tricornutum (Bacillariophyceae) stressed by iron. *BioMetals*, 17, pp.45–52.

Kremp, A., Tamminen, T. & Spilling, K., 2008. Dinoflagellate bloom formation in natural assemblages with diatoms: nutrient competition and growth strategies in Baltic spring phytoplankton. *Aquatic Microbial Ecology*, 50(2), pp.181–196.

Kurekin, A.A., Miller, P.I. & Van der Woerd, H.J., 2014. Satellite discrimination of Karenia mikimotoi and Phaeocystis harmful algal blooms in European coastal waters: merged classification of ocean colour data. *Harmful Algae*, 31, pp.163–176.

Lazzara, L., Bricaud, A. & Claustre, H., 1996. Spectral absorption and fluorescence excitation properties of phytoplanktonic populations at a mesotrophic and an oligotrophic site in the tropical North Atlantic (EUMELI program). *Deep-Sea Research Part I: Oceanographic Research Papers*, 43(8), pp.1215–1240.

Lewis, M.R., Cullen, J.J. & Platt, T., 1984. Relationships between vertical mixing and photoadaptation of phytoplankton: similarity criteria. *Marine Ecology Progress Series*, 15, pp.141–149.

Li, W.K.W. et al., 1983. Autotrophic picoplankton in the tropical ocean. *Science*, 219, pp.292–295.

Linacre, L. et al., 2015. Distribution pattern of picoplankton carbon biomass linked to mesoscale dynamics in the southern gulf of Mexico during winter conditions. *Deep Sea Research Part I: Oceanographic Research Papers*, 106, pp.55–67.

Liu, H. et al., 2009. Extreme diversity in noncalcifying haptophytes explains a major pigment paradox in open oceans. *Proceedings of the National Academy of Sciences*, 106(31), pp.12803–12808.

Lohrenz, S.E., Weidemann, A.D. & Tuel, M., 2003. Phytoplankton spectral absorption as in uenced by community size structure and pigment composition. *Journal of Plankton Research*, 25(1), pp.35–61.

Longhurst, A.R., 1998. *Ecological Geography of the Sea*, Academic Press.

Lorenzen, C.J., 1966. A method for the continuous measurement of in vivo chlorophyll concentration. *Deep Sea Research and Oceanographic Abstracts*, 13(2), pp.223–227.

Lutz, V.A., Sathyendranath, S. & Head, E.J.H., 1996. Absorption coefficient of phytoplankton: Regional variations in the North Atlantic. *Marine Ecology Progress Series*, 135(1-3), pp.197–213.

Maclsaac, E.A. & Stockner, J.G., 1993. Enumeration of phototrophic picoplankton by autofluorescence microscopy. In P. F. Kemp et al., eds. *Handbook of Methods in Aquatic Microbial Ecology*. Florida, USA: CRC Press, pp. 187–198.

Massana, R., 2011. Eukaryotic picoplankton in surface oceans. *Annual Review of Microbiology*, 65(May), pp.91–110.

Matsuoka, A. et al., 2009. Phytoplankton community adaptation to changing light levels in the southern Beaufort Sea, Canadian Arctic. *Estuarine, Coastal and Shelf Science*, 82(3), pp.537–546.

Miller, P.I. et al., 2006. SeaWiFS discrimination of harmful algal bloom evolution. *International Journal of Remote Sensing*, 27(11), pp.2287–2301.

Le Moigne, F.A.C. et al., 2015. Carbon export efficiency and phytoplankton community composition in the Atlantic sector of the Arctic Ocean. *Journal of Geophysical Research: Oceans*, 120(6), pp.3896–3912.

Moore, C.M. et al., 2013. Processes and patterns of oceanic nutrient limitation. *Nature Geoscience*, 6(9), pp.701–710.

Moore, L.R., Goericke, R. & Chisholm, S.W., 1995. Comparative physiology of Synechococcus and Prochlorococcus: influence of light and temperature on growth, pigment, fluorescence and absorptive properties. *Marine Ecology Progress Series*, 116, pp.259–275.

Morel, A., 2008. Introduction to optical properties in the sea: theoretical aspects. In M. Babin, C. S. Roesler, & J. J. Cullen, eds. *Real-time Coastal Observing Systems for Ecosystem Dynamics and Harmful Algal Blooms*. Paris, France: UNESCO Publishing, pp. 109–151.

Morel, A. et al., 1993. Prochlorococcus and Synechococcus: a comparative study of their size, pigmentation and related optical properties. *Journal of Marine Research*, 51, pp.617–649.

Morel, A. & Bricaud, A., 1986. Inherent optical properties of algal cells including picoplankton: theoretical and experimental results. *Canadian Bulletin of Fisheries and Aquatic Science*, 214, pp.521–559.

Morel, A. & Bricaud, A., 1981. Theoretical results concerning light-absorption in a discrete medium, and application to specific absorption of phytoplankton. *Deep-Sea Research Part a-Oceanographic Research Papers*, 28(11), pp.1375–1393.

Morel, A. & Maritorena, S., 2001. Bio-optical properties of oceanic waters: A reappraisal. *Journal of Geophysical Research: Oceans*, 106(C4), pp.7163–7180.

Mullin, M.M., 1965. Size fractionation of particulate organic carbon in the surface waters of the Western Indean Ocean. *Limnology and Oceanography*, pp.459–462.

Murphy, J. & Riley, J.P., 1962. A modified single solution method for the determination of phosphate in natural waters. *Analytica Chimica Acta 31*, 27(27), pp.31–36.

Nair, A. et al., 2008. Remote sensing of phytoplankton functional types. *Remote Sensing of Environment*, 112(8), pp.3366–3375.

Okolodkov, Y.B., 2003. A review of Russian plankton research in the Gulf of Mexico and the Caribbean Sea in the 1960-1980s. *Hidrobiológica*, 13(3), pp.207–221.

Partensky, F., Hess, W.R. & Vaulot, D., 1999. Prochlorococcus, a marine photosynthetic prokaryote of global significance. *Microbiology and Molecular Biology Reviews*, 63(1), pp.106–127.

Platt, T. et al., 2005. Physical forcing and phytoplankton distributions. *Scientia Marina*, 69, pp.55–73.

Prieur, L. & Sathyendranath, S., 1981. An optical classification of coastal and oceanic waters based on the specific spectral absorption curves of phytoplankton pigments, dissolved organic matters, and other particulate materials. *Limonology And Oceanography*, 26(4), pp.671–689.

Le Quéré, C. et al., 2005. Ecosystem dynamics based on plankton functional types for global ocean biogeochemistry models. *Global Change Biology*, 11(11), pp.2016–2040.

Raimbault, P. et al., 1990. Feasibility of using an automated colorimetric procedure for the determination of seawater nitrate in the 0 to 100 nM range: examples from field and culture. *Marine Biology*, 104(2), pp.347–351.

Ras, J., Claustre, H. & Uitz, J., 2008. Spatial variability of phytoplankton pigment distributions in the Subtropical South Pacific Ocean: comparison between in situ and predicted data. *Biogeosciences*, 5, pp.353–369.

Robertson, J.E. et al., 1994. The impact of a coccolithophore bloom on oceanic carbon uptake in the northeast Atlantic during summer 1991. *Deep-Sea Research Part I*, 41(2), pp.297–314.

Runge, J.A. & Ohman, M.D., 1982. Size Fractionation of phytoplankton as an estimate of food size fractionation available to herbivores. *Limnology and Oceanography*, 27(3), pp.570–576.

Sakshaug, E. & Slagstad, D., 1991. Light and productivity of phytoplankton in polar marine ecosystems: a physiological view. *Polar Research*, 10(1), pp.69–85.

Sarmiento, J.L. & Gruber, N., 2006. *Ocean Biogeochemical Dynamics*, New Jersy, USA: Princeton University Press.

Sarthou, G. et al., 2005. Growth physiology and fate of diatoms in the ocean: a review. *Journal of Sea Research*, 53, pp.25–42.

Sathyendranath, S., Lazzara, L. & Prieur, L., 1987. Variations in the spectral values of specific absorption of phytoplankton. *Limnology and Oceanography*, 32(2), pp.403–415.

Sathyendranath, S. & Platt, T., 2007. Spectral effects in bio-optical control on the ocean system. *Oceanologia*, 49(1), pp.5–39.

Sauzède, R. et al., 2015. Vertical distribution of chlorophyll a concentration and phytoplankton community composition from in situ fluorescence profiles: a first database for the global ocean. *Earth System Science Data*, 7(2), pp.261–273.

Shen, P. et al., 2011. Phaeocystis globosa Scherffel, a harmful microalga, and its production of dimethylsulfoniopropionate. *Chinese Journal of Oceanology and Limnology*, 29(4), pp.869–873.

Sieburth, J.M., Smetacek, V. & Lenz, J., 1978. Pelagic ecosystem structure: heterotrophic compartments of the plankton and their relationship to plankton size fractions. *Limnology and Oceanography*, 23(6), pp.1256–1263.

Silsbe, G.M. & Malkin, S.Y., 2015. phytotools: Phytoplankton Production Tools.

Smayda, T.J., 1971. Normal and accelerated sinking of phytoplankton in the sea. *Marine Geology*, 11(2), pp.105–122.

Sosik, H.M., 1996. Bio-optical modeling of primary production: consequences of variability in quantum yield and specific absorption. *Marine Ecology Progress Series*, 143(1-3), pp.225–238.

Sosik, H.M., 2008. Characterizing seawater constituents from optical properties. In M. Babin, C. S. Roesler, & J. J. Cullen, eds. *Real-time Coastal Observing Systems for Ecosystem Dynamics and Harmful Algal Blooms*. Paris, France: UNESCO Publishing, pp. 281–329.

Sosik, H.M. & Mitchell, B.G., 1991. Absortion, fluorescence, and quantum yield for growth in nitrogen-limited Dunaliella tertiolecta. *Limnology and Oceanography*, 36(5), pp.910–921.

Sosik, H.M. & Mitchell, B.G., 1995. Light absorption by phytoplankton, photosynthetic pigments and detritus in the California Current System. *Deep-Sea Research Part I*, 42(10), pp.1717–1748.

Stefels, J. & van Boekel, W.H.M., 1993. Production of DMS from dissolved DMSP in axenic cultures of the marine phytoplankton species Phaeocystis sp. *Marine Ecology Progress Series*, 97, pp.11–18.

Stramski, D., Sciandra, A. & Claustre, H., 2002. Effects of temperature, nitrogen, and light limitation on the optical properties of the marine diatom Thalassiosira pseudonana. *Limnology And Oceanography*, 47(2), pp.392–403.

Stuart, V. et al., 2000. Bio-optical characteristics of diatom and prymnesiophyte populations in the Labrador Sea. *Marine Ecology Progress Series*, 201(1991), pp.91–106.

Stuart, V. et al., 1998. Pigments and species composition of natural phytoplankton populations: effect on the absorption spectra. *Journal of Plankton Research*, 20(2), p.187; 187–217; 217.

Switzer, A.C., Kamykowski, D. & Zentata, S.-J., 2003. Mapping nitrate in the global ocean using remotely sensed sea surface temperature. *Journal of Geophysical Research*, 108(C8), p.3280.

Taylor, F.J.R., Hoppenrath, M. & Saldarriaga, J.F., 2008. Dinoflagellate diversity and distribution. *Biodiversity and Conservation*, 17(2), pp.407–418.

Tréguer, P. et al., 1995. The silica balance in the world ocean: a reestimate. *Science*, 268(5209), pp.375–9.

Turner, S.M. et al., 1988. The seasonal variation of dimethyl sulfide and dimethylsulfoniopropionate concentrations in nearshore waters. *Limnology and Oceanography*, 33(3), pp.364–375.

Tyrrell, T., Holligan, P.M. & Mobley, C.D., 1999. Optical impacts of oceanic coccolithophore blooms. *Journal of Geophysical Research*, 104(C2), p.3223.

Uitz, J. et al., 2009. A phytoplankton class-specific primary production model applied to the Kerguelen Islands region (Southern Ocean). *Deep-Sea Research Part I: Oceanographic Research Papers*, 56(4), pp.541–560.

Uitz, J. et al., 2006. Vertical distribution of phytoplankton communities in open ocean: An assessment based on surface chlorophyll. *Journal of Geophysical Research: Oceans*, 111(8).

Veldhuis, M.J.W. & Kraay, G.W., 2004. Phytoplankton in the subtropical Atlantic Ocean: towards a better assessment of biomass and composition. *Deep Sea Research Part I: Oceanographic Research Papers*, 51(4), pp.507–530.

Vidussi, F. et al., 2001. Phytoplankton pigment distribution in relation to upper thermocline circulation in the eastern Mediterranean Sea during winter. *Journal of Geophysical Research*, 106, pp.939–956.

Wawrik, B. et al., 2003. Vertical structure of the phytoplankton community associated with a coastal plume in the Gulf of Mexico. *Marine Ecology Progress Series*, 251(3), pp.87–101.

Williams, R.G. & Follows, M.J., 2011. *Ocean Dynamics and the Carbon Cycle*, Cambridge, UK: Cambridge University Press.

Wood, E.D., Armstrong, F.A.J. & Richards, F.A., 1967. Determination of nitrate in sea water by cadmium-copper reduction to nitrite. *Journal of the Marine Biological Association of the UK*, 47(01), pp.23–31.

Woodward, E.M.S. & Rees, A.P., 2001. Nutrient distributions in an anticyclonic eddy in the northeast Atlantic ocean, with reference to nanomolar ammonium concentrations. *Deep-Sea Research Part II: Topical Studies in Oceanography*, 48(4-5), pp.775–793.

Yentsch, C.S. & Menzel, D.W., 1963. A method for the determination of phytoplankton chlorophyll and phaeophytin by fluorescence. *Deep Sea Research and Oceanographic Abstracts*, 10(3), pp.221–231.

Yentsch, C.S. & Phinney, D. a., 1989. A bridge between ocean optics and microbial ecology. *Limnology and Oceanography*, 34(8), pp.1694–1705.

Yoch, D.C., 2002. Dimethylsulfoniopropionate: its sources, role in the marine food web, and biological degradation to dimethylsulfide. *Applied and Environmental Microbiology*, 68(12), pp.5804–5815.

Yool, A. & Tyrrell, T., 2003. The role of diatoms in regulating the ocean's silicate cycle. *Global Biogeochemical Cycles*, 17(4), pp.1–24.